

Erosion-Corrosion: An Up-To-Date Review of Origin, Impacts, Affecting Factors, Occurrence Areas, Experimental Measuring Devices, and Research Advances

TN Guma, DD Ishaya, EA Abhulimen, and SO Yakubu

Department of Mechanical Engineering, Faculty of Engineering and Technology, Nigerian Defence Academy, Kaduna, Nigeria

DOI : <https://doi.org/10.51583/IJLTEMAS.2024.131212>

Received: 16 December 2024; Accepted: 24 December 2024; Published: 09 January 2025

Abstract: An up-to-date review of erosion-corrosion from various literary sources, covering its origin, impacts, affecting factors, occurrence areas, experimental measuring devices, and research advances, is reported. From the review, erosion-corrosion is a mechanically caused action by impinging fluid, usually liquid, slurry abrasion, suspended particles in fast-flowing fluids, bubbles, droplets, cavitations, etc., under complex synergistic effects of the natural electrochemical corrosion. It is affected by many factors that still need to be fully understood, so it is very challenging to accurately find its rates for controlling it. It is a very costly problem that is common in power plants, water, oil, gas, metallurgy, mining, and other industrial sectors that utilize mechanical equipment as well as structural components in hydraulic environments. Its effects are predominant in petroleum pipelines and heat exchange industries, as well as marine equipment or structures. Its rates, time scale, and capacity to degenerate material components to failure are much more alarming than most other corrosion types. This corrosion type is highly detestable, so much attention has been drawn to it, as attested by many research outputs on it to date, with a pressing need for ways, including emerging technologies, of minimizing its impacts. Forty-six of the research outputs have been recapitulated and presented, and they focus on developing and/or testing alternative material components, coatings, measuring devices, and application of artificial intelligence, for better erosion-corrosion resistances or rate measurements and control under various fluid conditions. The paper provides integrated, up-to-date information on erosion-corrosion for easy accessibility for the needful basic knowledge for research progress towards reducing its impacts.

Keywords: Erosion-corrosion, Affecting factors, Rates determination, Measuring devices, Challenges, Emerging technologies, Research advances, Up-to-date information

A Glossary of some Technical Terms

Anodic polarization: An electrochemical technology that allows thick and opportunely structured metal oxide films over the surface of a metal to be obtained.

Artificial intelligence (AI): A set of technologies that enable computers to perform a variety of advanced functions, including the ability to see, understand, and translate spoken and written language; analyze data; make recommendations; and do other things on their own to accomplish tasks that humans cannot ordinarily do.

Cermet: A composite material consisting of ceramic and metallic materials.

Computational Fluid Dynamics (CFD): The analysis of fluid flows using numerical solution techniques.

Dissolved oxygen (DO) probe: Technique or facility used for measuring the amount of dissolved oxygen in an aqueous medium

Electrochemical Impedance Spectroscopy (EIS): An electrochemical technique used in corrosion analysis and other areas like fuel cell development, sensor development, battery development, and physical electrochemistry. And paint characterization.

Emerging technologies: Technologies that are generally new whose development, and/or practical applications are still largely unrealized but are finding new applications with impactful results.

Focused ion beam (FIB): A device or method used in combination with the scanning electron microscope for both imaging and preparation of a wide range of solid sample types.

Metallography: The study of the physical microstructure of metals and alloys, often via microscopy analysis for understanding the mechanical properties of materials, such as their grain size, crystal structure, and the presence of any defects such as cracks or non-metallic inclusions.

Micro-cutting, very tiny, invisible cutting of material by corrosive agents

Microstructure: Material structures that can only be seen at the micro level using high-magnification imaging facilities.

Passivation: The natural formation process of a protective layer on a metal or the use of a light coat of a protective material, such as metal oxide, to create a layer against corrosion.

Polarization: The distortion of a negatively charged electron cloud by a positively charged ion.

Morphology: The study of the microstructure of metals.

Potentiodynamic polarization: An electrochemical technique where the potential is increased or decreased with time in a linear way while the current is recorded.

Potentiostatic Polarization: A simple, widely used electrochemical measurement technique Scanning Electron Microscopy (SEM): A method of material analysis by spectroscopy technique that uses the principle of light microscopy to create a form of high-resolution surface imaging Scanning transmission electron microscopy (STEM): An analytical microscope that is based on the combination of SEM and TEM, for which scanning method is used to obtain a transmission image.

Transmission electron microscopy (TEM): An analytical microscopy or microscope used for visualizing the smallest structures in matter by magnifying nanometer structures up to 50 million times.

Slurry: A mixture of fluid and solid particles that cause metal or material erosion-corrosion.

I. Introduction

Corrosion is a natural process of destructive attack on a material, particularly metal, caused by electrochemical and physical interactions between the material and its surroundings [1]. The attack can manifest in degrading the material by appearance, microstructure, weight loss, and reduction in cherished values of its mechanical and physical properties such as strength, hardness, thermal and electrical conductivity, etc. that should be preserved [1, 2, 3]. The consequences of corrosion in its entirety are globally economically monumental, and technologically encompassing. These consequences directly or indirectly affect every human being, village, community, nation, and the world over. The total combined direct and indirect global cost of corrosion menacing every facet of our economy and engineering technology in our industrial era, is estimated to be 2.5 trillion dollars yearly, equivalent to about 3.4% of the world's yearly gross domestic product [4, 5].

There are various types of corrosion. Erosion-corrosion is a type of corrosion that is due to the combined action of the pure natural electrochemical corrosion process and wear by mechanical action of fluid flow. In other words, it is a corrosion phenomenon that causes material degradation by electrochemical corrosion and wear processes in moving fluids. The detestation about erosion-corrosion is that its rates, time scale, and capability to cause failure of material components are much more alarming than most other corrosion types. It is a very serious common problem in power plants, water, oil, gas, metallurgy, mining, and other industrial sectors that utilize mechanical equipment as well as other material components in hydraulic environments. [6, 7, 8] The sources of the various mechanical forces that cause erosion include turbulent flow, fluctuating shear stress and pressure impacts, the impact of suspended solid particles, the impact of suspended liquid droplets in high-speed gas flow, the impact of suspended gas bubbles in aqueous flow, and the violent collapse of vapor bubbles following cavitation. Impingement erosion-corrosion involving slurry particles is a common phenomenon with a great destructive impact on flow components such as pump impellers, pipelines, elbows, hydro-turbines, and choke valves or nozzles in many engineering fields. Because this corrosion type is so complex and its affecting factors fluctuate wildly and unpredictably with fluid conditions, it is exceedingly challenging and unreliable to accurately forecast its rates and other effects using the developed models on it in order to extend the in-service lives of equipment and other material components. However, precise information on the corrosion's origins, rates, impacts, affecting factors, occurrence areas, experimental measuring devices, and research findings is necessary for developing the overall strategies of controlling it and advancing the field of research on it [9, 10, 11].

Because of the high vulnerability and complex nature of erosion-corrosion, necessitating the need to develop better methods of combating it, it has drawn a lot of research attention in recent years [8-15]. Various methods with different advantages and limitations, such as design modifications, routine maintenance and inspection, reduction of suction pipe lengths, alteration of fluid environments to minimize flow velocity and turbulence, provision of cathodic protection, reduction of the pipe joints number, use of strainers and filters to minimize contaminants in fluids, etc., are often exploited in industries to prevent or minimize its effects, but the use of corrosion-resistant materials that are compatible with the various prevailing environments and the use of coatings and other surface treatments have greater impact with long-term performance implications and cost-effectiveness than the other methods. For effectiveness and reliability of a chosen protective method against erosion-corrosion of a material in a given environment, knowledge of accurate environmental corrosion rates of the material in that environment is necessary for optimal implementation of the method. Erosion-corrosion rates of materials are, however, usually test-evaluated using conventional methods. Conventional methods of determining erosion-corrosion rates and their other effects, for optimal control or research purposes, involve the use of special testing rigs or devices, classical detection techniques such as visual inspections, weight loss, radiographic testing, and ultrasonic testing, and electrochemical techniques such as potentiodynamic polarization and electrochemical impedance spectroscopy (EIS). However, such devices or rigs are often not available, affordable, or known for the corrosion measurement in many laboratories or locations, especially in developing countries such as Nigeria. Moreover, the conventional approaches to erosion-corrosion monitoring and research can yield accurate and useful information on its environmental rates, these approaches are usually labor-intensive and time-consuming, and they may not be able to identify corrosion in its early stages or offer thorough information on the distribution and severity of corrosion in an environment. Also, the available mechanistic, empirical, and semi-empirical models for predicting the corrosion rates and their other effects lack

clear validity and reliability for use in industries. More sophisticated and flexible methods are therefore required to handle the erosion-corrosion of its complex nature [7, 8, 16, 17]. A thorough approach to complex corrosion analysis of material components is provided by emerging technologies, particularly artificial intelligence, with capabilities in machine learning, data analysis, and pattern recognition for processing large amounts of data and recognizing intricate patterns to produce or predict more precise and timely information on corrosion rates of material components even in unsafe and intricate environments for enabling proactive maintenance and lowering the risk of catastrophic failures [6].

The aim of this paper is to provide an up-to-date review report on erosion-corrosion from various reputable literary sources covering its origin, impacts, affecting factors, occurrence areas, experimental measuring devices, and research advances, including insights into the emerging technologies, especially artificial intelligence and machine learning, as integrated information for easy accessibility by the relevant students, researchers, engineers, practitioners, stakeholders, and scientists for the needful basic knowledge for research strategies towards its optimal control to reduce its impacts.

II. Methodology

The review information on erosion-corrosion was sourced from various current relevant books, journals, theses, and other reputable literal sources published from 2014 to 2024 in hard or soft copy forms which are available in institutional libraries and on the Internet, recapitulated, integrated, and fine-tuned for enhanced readability, and better understanding.

III. The Review Report

Background Information on Erosion-Corrosion

By comparison to erosion and corrosion alone, the erosion-corrosion process is extremely complex. The processes of erosion and corrosion differ significantly depending on whether gases and solids are present or not. The mechanism of erosion and corrosion is difficult to explain because of all the many variables and the several processes that are going on at the same time. Many industrial sectors, including the maritime, oil and gas, nuclear, high-temperature, power generation, mining, and process industries, are significantly impacted by erosion and corrosion. Furthermore, it is impossible to overlook how erosion and corrosion affect the aerospace, food, mining, and dental industries. The total cost of erosion-corrosion in numerous industrial processes is several hundreds of millions of dollars annually, including lumping together plant shutdowns, replacing worn-out equipment, decreased process efficiencies, production loss and contamination, over-design practices, and the implementation of safety factors. Equipment that must be in contact with the marine environment should have excellent resistance to corrosion. Many environments, such as marine water, offer aggressive erosion and corrosion to the materials with which it interacts. Chloride contents of the sea or other waters are more prone to pitting corrosion, and sand present in such water environments accelerates erosion and corrosion. Moveable components present in marine equipment unavoidably suffer from corrosion and wear. The degradation of material components by erosion and corrosion has a great impact on safety, economy, and contamination in industrial sectors. The degradation of material components by erosion and corrosion is depicted in Fig. 1 [6, 7, 8].

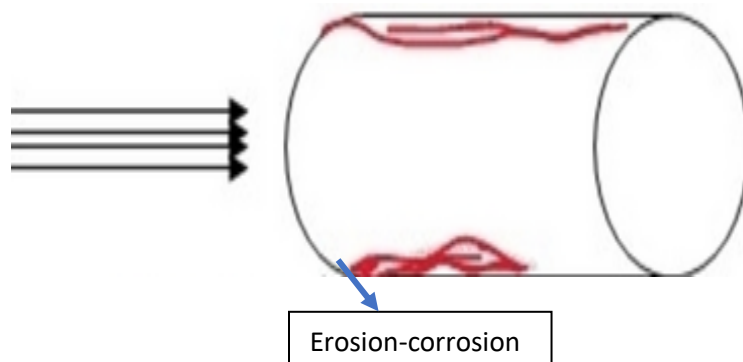


Fig. 1: Degradation of material component by erosion-corrosion [8]

Slurry erosion-corrosion occurs when a fluid that contains solid particles interacts with a target surface, which then experiences a loss of material. Solid particles may vary in diameter, shape, and concentration depending on the nature of the slurry flow. Slurry could be either settling or non-settling, which depends on the flow dynamics of the liquid. Although slurry erosion-corrosion consideration is used in design and other corrosion preventive methods of engineering structures used in many fluid flow applications, the corrosion is inevitable, for it can only be alleviated or prevented for a specified time but not permanently [6, 7]. The corrosion of material components in such applications can still be accelerated to inimical levels by unpredictable fluid flow conditions and mechanical effects resulting from solid-phase matters. Optimal impingement erosion-corrosion prevention of material components used in such applications is of great concern to engineers considering the imminent disastrous consequences [6, 7, 8]. Optimal impingement erosion-corrosion relies greatly on test data from field operating conditions, service operating conditions, and laboratory-simulated operating conditions. Data obtained from laboratory-simulated operating conditions is cheaper to obtain and is the first step in considering the suitability of a material component for application in field and service

applications or tests, considering the enormous cost that is often associated with the other tests. Although test data have been provided by research that can be exploited for impingement erosion-corrosion prevention of material components under different flow operating conditions, applicable information is still greatly lacking for all the numerous unpredictable water flow conditions that can cause inimical erosion-corrosion in various types of material components. Such essential information is required for all the countless water and other fluid flow conditions and is needed the world over for strategies in impingement erosion-corrosion control and management [6, 7, 8].

Generally, almost all components moving near a corrosive fluid hitting the material surface are exposed to corrosive erosion. Transmission pipes for gas, oil, and water, as well as the transmission lines for fluid in the industrial reactor, and heat exchange systems suffer significantly from the erosion-corrosion phenomenon. Erosion-corrosion can generate material loss much greater than the sum of the pure erosion and the pure corrosion individually due to the interplay between them. Erosion-corrosion in aqueous systems is dominated by two major mechanisms: electrochemical corrosion and mechanical erosion. In general, the influencing parameters in this process include the solid sand particles by mass, hardness, density, size, shape, velocity, and impact angle; the target material's hardness, metallographic structure, strength, ductility, and toughness; and the environment slurry composition, flow velocity, and temperature [9]. Degradation of materials due to slurry erosion-corrosion depends on many factors, which can be divided into three main groups: the first group is connected to fluid flow conditions such as flow velocity, angle of liquid and particle impingement, particle concentration, liquid density, liquid chemical activity, and liquid temperature [10, 11, 12]. The second group is connected with the nature of solid particles in terms of size, shape, hardness, and strength. The third group is connected to the endurance and mechanical properties of the target material.

In erosion-corrosion, there are three separate phenomena: the impact of solid particles on the surface of the material, electrochemical reactions, and the fluidity of the medium. These processes interact with each other and create erosive corrosion, forming a completely complex phenomenon. The interaction between erosion, corrosion, and the fluid environment is depicted in Fig. 2. This shows that the erosive corrosion process can only exist if erosion, corrosion, and the fluid environment exist at the same time [7, 8, 10].

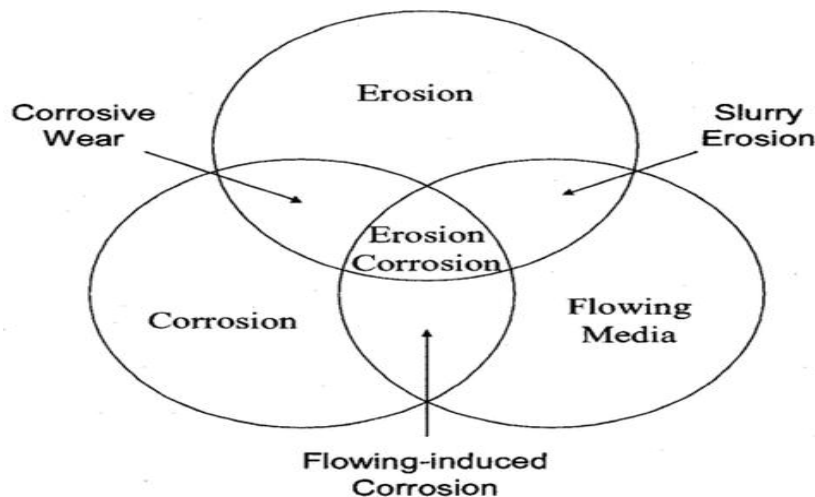


Fig. 2: Schematic representation of the interaction of erosive corrosion phenomena [8, 10].

Effects of Impingement Erosion-corrosion

Impingement erosion-corrosion usually produces a pattern of localized attack with directional features on solid materials [6, 7]. Particles of sand or other particles impinging on the pipe wall surface can remove the protective iron carbonate scale or prevent it from adhering to the pipe and other material walls. This can expose bare metal to corrosive environments at these impingement points and lead to unacceptably high corrosion rates [7, 8, 9]. The main effects of impingement corrosion are economic losses resulting from the need to replace or regenerate machinery or facilities and stop the technological process. Erosion-corrosion causes gradual mass loss of the surface layer, changing the geometry of the elements of the installations and machinery, which leads to a reduction in their efficiency and service life [10, 11, 12]. The costs of failures associated with impingement erosion-corrosion are real business problems that stem from replacements or regeneration of eroded machine parts, loss of productivity, indirect losses of energy, and increased environmental burden [12, 13]. Aqueous fluid flow impingement can cause severe erosion and corrosion in the oil and gas production and hydropower industries, resulting in economic penalties such as catastrophic component failure, increased downtime, and increased maintenance costs [7, 8, 12, 13].

Factors Affecting Impingement Erosion Corrosion

The erosion-corrosion performance of material components in a fluid is affected by a wide range of factors, such as environmental conditions, target component properties, and particle concentration, size, shape, velocity, kinetic energy, etc., as shown in Fig. 3. Important particle properties are hardness, shape, size, and density. Impingement angle, impact velocity, slurry

concentration, environment composition, and temperature fall under environmental factors. Target component properties include toughness, microstructure, hardness, and strength. Some of the factors, such as chemical composition, temperature, salinity, dissolved oxygen, and pH, generally affect corrosion more than erosion. Factors such as velocity, impact angle, particle size, and mechanical properties of materials have a greater influence on pure erosion than corrosion, but all of the factors have effects on corrosion and erosion in a complex, synergistic manner [8, 15, 16]. All the factors influencing erosion, corrosion, and the synergistic effect of pure mechanical erosion and electrochemical corrosion are so complex and interwoven that they still need to be fully investigated individually and in various combinations for better understanding of the erosion-corrosion mechanism and effects [8, 9].

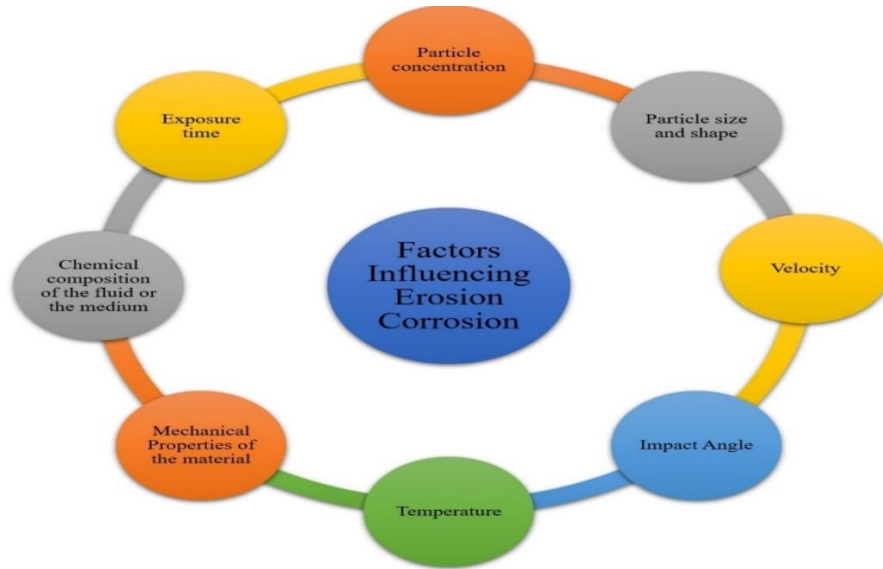


Fig. 3: Factors that affect the impingement erosion-corrosion [8]

Insight into Models for Erosion-corrosion

Many models have been proposed to characterize factors affecting erosion-corrosion but the models are too complex and many for accurately predicting the erosion behavior under various fluid flow conditions [9,16]. For example, it is proposed that the ratio of the eroded material volume to the volume of the craters formed during erosion-corrosion could be presented as an erosion efficiency parameter (η) that can be expressed as given in Eq. 1 [9].

$$\eta = \frac{2H_T V}{M_p V_p^2} \dots \dots \dots (1)$$

Where H_T is the Vickers microhardness of the target material, V is the volume of removed material (m^3), and M_p (kg) and V_p (m/s) are the mass and velocity of the particle, respectively. In the case of normal impact erosion, it has been suggested that the brittle mechanism is dominant when $\eta > 1$, whereas deformation controls the erosion mechanism if $\eta < 1$

By considering the required and expended energy for the material removal, Eq. (1) is extended and an erosion mechanism identifier (ξ) introduced for predicting the erosion mechanism under both oblique and normal impact as by Eq. 2.

$$\xi = \frac{2V \sigma_{cr} \left(\frac{H_T}{K_T} \right)}{M_p V_p^2} \dots \dots \dots (2)$$

Where V , H_T , M_p , and V_p have the same meanings as in Eq. (1); K_T is a material toughness (MPa) and σ_{cr} is a critical stress (MPa) that depends on the type of material. For brittle metals and alloys, σ_{cr} is considered to be equal to the ultimate tensile strength whereas for ductile materials, σ_{cr} is taken as equivalent to the ultimate shear stress of the material. It has been proposed that the dominant erosion mode is ploughing if $\xi < 1$, micro-cutting if $\xi = 1$, and brittle if $\xi > 1$ [9].

The effect of particle shape on erosion is quantified by defining the particle circularity through the shape factor (S_F) given by Eq. (3).

$$S_F = \frac{4\pi A_p}{p^2} \dots \dots \dots (3)$$

where, A_p is the projected impact area (m^2) and P is the overall perimeter (m) of the projection of a solid particle. The particle perimeter can be evaluated on the basis of the measured length (L_p) and width (W_p) of the particle, given by Eq. (4) [9], as,

$$P = \frac{\pi}{2} \left[\frac{3}{2} (L_P + W_P) - \left(\frac{L_P}{W_P} \right)^{\frac{1}{2}} \right] \dots \dots \dots (4)$$

For a circular particle, the shape factor is equal to one and any deviation away from one indicates a departure from circularity. Thus, the lower the value of the shape factor, the higher the angularity of the particles. Due to the high standard deviation observed for many particle measurements, a modified shape factor is (MS_F) is given by Eq. 5.

$$MS_F = \left[(SF)_{Avg} (SF)_{Min} (SF)_{Max} \right]^{\frac{1}{3}} \dots \dots \dots (5)$$

where $(SF)_{Avg}$ is the average value of all measurements, and $(SF)_{min}$ and $(SF)_{max}$ are the minimum and maximum values of SF [9].

Erosion increases with an increase in the slurry particle (flow) velocity. Many researchers have proposed that the erosion rate (E_R) exhibits an empirical power law relationship with the erosive particle velocity according to Eq. (6).

$$E_R = KV_p^m \dots \dots \dots (6)$$

where E_R is the erosion rate, V_p is the velocity of the solid particles (m/s), K is an empirical constant, and m is the velocity exponent varying from 0.34 to 4.83 depending upon the particle and material properties and condition of the test. The values of K have been reported for some materials under specific conditions [9].

If the particles are more or less spherical with a diameter d_p and density ρ_p , travelling with a velocity of V_p , their kinetic energy Φ is simply given by Eq. 7.

$$\Phi = \frac{\pi \rho_p d_p^3 V_p^2}{12} \dots \dots \dots (7)$$

The second stage of material erosion is caused by fragmented particles projected radially on the primary scars. For any impact angle, the total erosion rate, expressed as the material removed by unit mass of impacting particles, has been suggested by introducing a standard test reference velocity (V_{Ref}) and threshold velocity (V_{tsh}) below which distortion is entirely elastic and no erosion occurs to be the sum of the two proposed stages, as given in Eq. (8) [9].

$$E_R = \epsilon_1 \left(\frac{V_p}{V_{Ref}} \right)^2 \left[1 - \left(\frac{d_{tsh}}{d_p} \right)^{3/2} \frac{V_{tsh}}{V_p} \right]^2 + \epsilon_2 \left(\frac{V_p}{V_{Ref}} \right)^2 F_d \cdot V \dots \dots \dots (8)$$

where ϵ_1 and ϵ_2 are the maximum erosion (mg/g) for the reference velocity (m/s) of each stage, d_{tsh} is the threshold particle size (μm) below which no erosion damage occurs and, $F_d \cdot V$ is the degree of fragmentation, which is a function of particle size and velocity. $F_d \cdot V$ can be determined from Eq. 9 [9]:

$$F_d \cdot V = \frac{W_0 - W_1}{W_0} \dots \dots \dots (9)$$

It has been noteworthy from the literature that the development of erosion-corrosion models has been ongoing for the last three and a half decades. From the foregoing few exemplified models and many others from the literature, it is apparent that the models for predicting the erosion-corrosion rates and other effects are theoretical with many simplification assumptions, approximations, or generalizations without much clear information on their validity and practicability. There is therefore still a need for well-validated and time-tested worldwide-acceptable models on erosion-corrosion for use by industries with reliable practical results [9, 17].

Mechanisms of Impingement Erosion-Corrosion

The mechanism of erosion-corrosion results in the continual removal of the protective films responsible for the corrosion resistance of the material [10]. The sources of the various mechanical forces that cause erosion-corrosion include turbulent flow, fluctuating shear stress, and pressure impacts; the impact of suspended solid particles; the impact of suspended liquid droplets in high-speed gas flow; the impact of suspended gas bubbles in aqueous flow; and the violent collapse of vapor bubbles following cavitation. Impingement corrosion causes damage through various mechanisms [10]:

- i. Flow-accelerated corrosion (FAC).
- ii. Cavitation damage.
- iii. Erosion corrosion.

Impingement corrosion is commonly encountered in practice in fluid flow machinery, mainly in the hydropower industry and in the maritime industry, such as water turbines, valves, pipelines, and marine propellers. FAC is also termed flow-assisted corrosion. In this corrosion mechanism, the usually protective oxide layer on the surface of a metal is dissolved in fast-flowing

water through the formation and fast collapse of several small vapor bubbles, resulting in pits on the metal surface. The underlying metal corrodes and recreates the oxide in a vicious cycle with continued metal loss. In cavitation damage, the metal or material surface is damaged via the formation and collapse of bubbles on it, while in erosion corrosion, the metal or material surface is damaged faster by the relative motion of the fluid environment and the metal surface. Figs. 4, 5, and 6 show some of the mechanisms of fluid impingement corrosion in practical situations.

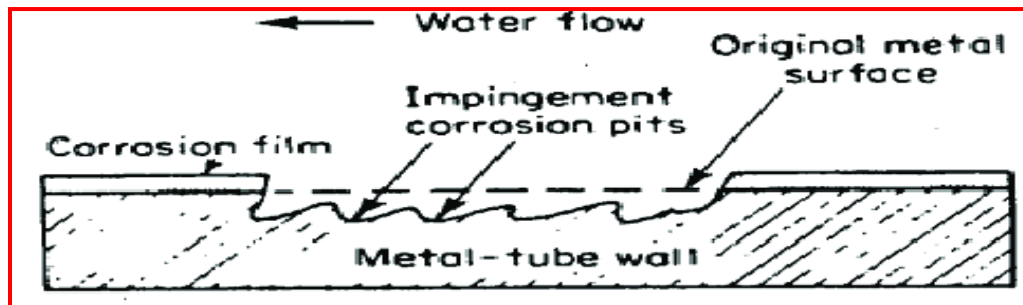


Fig. 4: Principle of impingement erosion corrosion of a straight metal tube [9, 10]

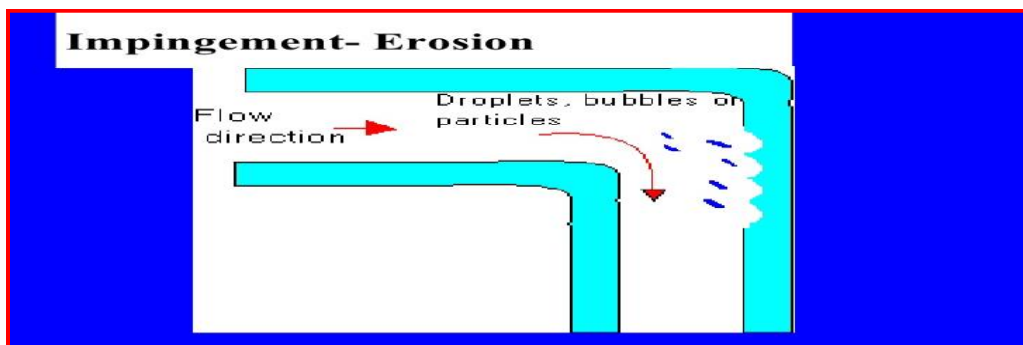


Fig. 5: Principle of impingement erosion-corrosion in a metal pipe near a 90°-degree angle bend [8, 10, 11]

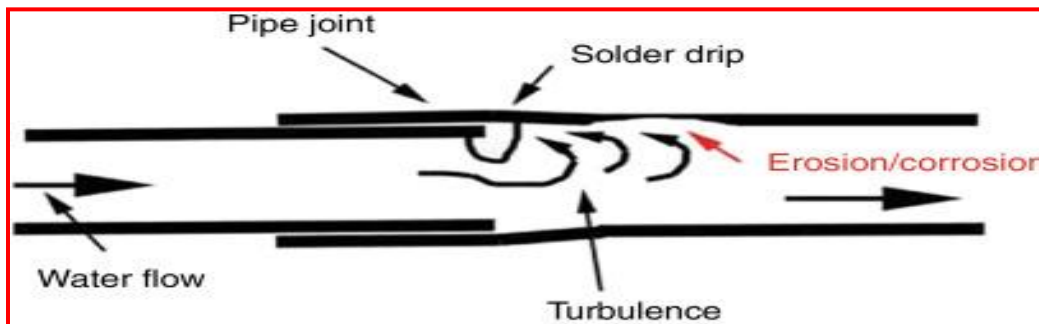


Fig. 6: Principle of impingement erosion corrosion in a metal pipe around a joint [7,8, 9]

The mechanical surface that is damaged by the impacting particle flow is caused by disruptive shearing forces and abrupt pressure changes on the material surface, which is sometimes coated with a protective layer. Deterioration is increased by solid particles and gas bubbles entrapped in the fluid, as well as the corrosive nature of the fluid in the working environment that reacts with the surface [9, 11].

The surface morphology affected by impingement corrosion may appear in the form of shallow pits, horseshoe patterns, or patterns related to local flow directions. The relative movement of a corrosive fluid and the metal's surface is responsible for impingement corrosion and damage to the surface. In the case of boiler tubes, for example, the turbulence due to initial pitting on the internal surface can result in accelerated corrosion and eventual tube leakage. Faulty manufacturing of tubes, such as burrs at smooth tube ends, can result in flow turbulence and high impingement velocities, thus causing severe impingement damage [7, 8, 9].

Insights into the use of Resistant Materials and Coatings to Erosion-corrosion

There are many methods of preventing erosion-corrosion, but the correct use of materials and coatings is probably the most convenient, effective, reliable, versatile, and popular method. Materials and coatings that are resistant to erosion-corrosion find diverse and successful applications in various industries such as oil and gas, hydropower, mining and mineral processing, solid waste landfill, marine, aerospace, automotive, and wastewater treatment. It is thus imperative to have basic insights into the

materials and coating types being used today to combat erosion-corrosion in various industrial settings engineering progress [16, 18, 19, 20].

Materials

Different classes of material types, such as metals, intermetallic alloys, composites, ceramic oxides, carbide ceramics, and nitride ceramics, are exploited with various benefits and limitations in industries to combat erosion-corrosion issues. The commonly exploited metals for erosion-corrosion protection, in order of their increasing effectiveness, are aluminum, nickel, zinc, tungsten, molybdenum, rhenium, niobium, cobalt, iron, and stainless steel. Intermetallic alloys are materials that are produced with an ordered mixture of at least two metallic elements to obtain more desirable properties than the individual metals. Intermetallic alloys are termed advanced materials due to their outstanding chemical, mechanical, optical, magnetic, electrical, and semiconducting properties. Nickel-aluminides, titanium aluminides, and molybdenum silicides are used to produce critical erosion-susceptible components of fluid machinery used in industries such as turbine blades [16, 18-22].

Composite materials are made by combining two or more unique materials to make a new material that surpasses its original components in engineering properties. These materials are widely employed in modern industries because of their outstanding properties. They generally don't corrode or rust. Numerous industries, including air pollution control, chemical processing, oil and gas, pulp and paper, desalination, food and beverage, mineral processing and mining, solid waste landfill, and water and wastewater treatment, can benefit from composites' corrosion-resistant solutions. Popular composites like fiberglass, carbon fiber, concrete, Kevlar, ceramic matrix, and metal matrix are exploited for various structural parts in industries such as the construction of wind turbines in renewable energy industries, construction of decks, boat hulls, structural columns, and other components in the marine industry. Carbon fiber is used for the construction of aircraft structural components such as fuselages, wings, and inside parts. Moreover, carbon fiber and fiberglass composites are used in almost everything from the body panels to the interior components of automotive vehicles to enhance their safety [16, 19-22].

Ceramic oxides are a class of advanced materials that are primarily characterized in their composition by metal elements bonded with oxygen. Ceramic oxides exhibit a wide range of outstanding properties, so they find wide applications in various industries. Ceramic oxides such as alumina (aluminum oxide), zirconia (zirconium oxide), magnesia (magnesium oxides), titania (titanium oxides), and chromium oxides are the most exploited to combat erosion-corrosion in various industries. Non-oxides ceramics such as all kinds of nitride (aluminum nitride, silicon nitride, and boron nitride), which are refractory but have very high durability under high temperatures as well as high corrosion and erosion resistance, are also selectable materials for many applications in industries involving erosion-corrosion. Because of their great hardness and remarkable resistance to high temperatures, abrasions, and corrosion, carbide ceramics, such as silicon carbide and boron carbide, and borides are potentially viable materials for erosion-corrosion prevention applications. They are mostly employed in mechanical, chemical, and power engineering; microelectronics; and space engineering due to their high thermal and changeable electrical conductivity [16, 18-22].

Coatings

Coatings provide protection by creating a physical shield between the substrate material and corrosive agent, sacrificing with a higher electrochemical potential than that of the underlying substrate to be protected, and offering an innovative self-healing mechanism. Raw material availability, application ease, affordability, adaptability, and versatility make coating the most popular, versatile, and successful protective technique. Coatings are frequently used in industries to prevent or mitigate erosion-corrosion to minimal levels, but not every coating type works well in every erosion-corrosion scenario; therefore, appropriate coatings must be chosen based on a variety of criteria, such as cost, efficacy, metal or other component types, and the environment corrosivity or aggressivity level. Selecting and applying the right coatings helps reduce erosion-corrosion damage and prolong the equipment's useful life. By comparison with coatings used in traditional applications, coatings for erosion-corrosion protection must have superior film strength, adhesion, curing time, flexibility, water resistance, abrasion resistance, and chemical resistance. In many different industries, coatings such as polyurethane, ceramic coatings, carbide and nitride coatings, and epoxy systems loaded with ceramic are frequently used to prevent or lessen erosion-corrosion [16-20]. A coating that must resist erosion-corrosion is typically examined and tested to meet many requirements such as [16-20]:

- i. Adequate coating bond strength
- ii. Adequate material density for the coating.
- iii. Adequate coating film hardness
- iv. Adequate resistance to erosion as per ASTM G76
- v. Adequate resistance to abrasion using Taber abrasion simulated tests
- vi. Sand jet test standard for resisting erosion by sand particles
- vii. Elasticity tests, such as impact tests and micro-penetration
- viii. Coating thickness uniformity.

- ix. Resisting cavitation erosion as per ASTM G32
- x. Water jet erosion measurement standard

Carbides are typically utilized for erosion-corrosion resistance and oxidation resistance. Tungsten carbide coatings, chromium carbide coatings, and titanium nitride coatings are examples of carbide and nitride coatings used to protect parts against erosion-corrosion. Tungsten carbide is deposited as a porous coating on metals using flame spray processes. Ceramics or polymers are used to fill porosity. The tungsten carbide is also coated onto component surfaces using the high-velocity oxy-fuel process. A thick deposit can be made on the substrate using a supersonic gas stream at high temperatures, and a very fine, polished layer can be achieved by honing and finishing this coating.

Ceramic and hard tungsten carbide coatings are also made by plasma coating. This method creates a stream of hot gas flame by partially ionizing argon gas with an electric arc. The hot gas flame is injected with ceramic powder, also known as tungsten carbide powder. Depending on how the component to be coated is configured, the plasma coating gun can be operated by robots or electronic controls. While chromium carbide coatings are used to prevent erosion at extremely high temperatures, titanium nitride is utilized to protect spacecraft and airplanes from erosion at low angles. Under severe erosion circumstances, tungsten carbide coatings offer erosion-corrosion protection at higher temperatures [16-20].

Advanced ceramic materials, such as oxide, carbide, nitride, and boride coatings, have been explored for erosion-corrosion protection due to their exceptional corrosion resistance. Thermal spray techniques like plasma spraying and high-velocity oxygen fuel (HVOF) spraying have been used to produce dense and uniform ceramic coatings with improved adhesion and corrosion resistance. Their remarkable performance in harsh environments, like high temperatures and erosion-corrosive conditions, makes them suitable for use in industries like energy, aerospace, and petroleum processing. The aviation industry makes considerable use of polymer-aluminum-ceramic coatings. These coatings protect the surfaces of aluminum alloys against rain erosion. In addition, they take the place of hard anodized layers, and they are applied as sealed coatings and work well against erosion and corrosion from raindrops. Instead of using dispersed cadmium-nickel coatings to coat the gas path components of aircraft, smooth, aerodynamic-sealed ceramic-aluminum coatings are employed. Ceramic coatings made of zirconium oxide are utilized in high-temperature applications, such as protecting hot gas turbine blade tips from erosion and corrosion, while aluminum oxide-ceramic coatings and chromium oxide-ceramic coatings are employed as cost-effective alternatives for erosion protection of light metal alloys. Cermet-based coatings are increasingly being used to contend with erosion-corrosion in oil and gas industries, such as in offshore piping, production systems, and equipment that involve fluid and/or slurry flowing in corrosive environments, which often contain sand and other solid particles. They are used to reduce erosion-corrosion in steam turbines and the issue of compressor fouling in ethylene gas handling systems, and hardened aluminum-ceramic coatings are utilized to reduce the erosion by hard particles in aquatic conditions. Chemicals handled at higher temperatures in the chemical and other process sectors are resistant to corrosion when coated with specially designed ceramics. When applied to steel surfaces instead of cadmium plating, metallic-aluminum-ceramic coating systems offer erosion protection in extremely acidic chemical environments, including SO₂ gas. They are applied as coatings to aluminum alloys and high-strength steels. Metal-filled polymers are used to protect the surfaces of magnesium and aluminum alloys from corrosion and erosion, and molybdenum disulfide (MoS₂) is used for anti-seize and erosion prevention purposes [16-22].

Epoxy resins are utilized in the automotive, chemical, oil and gas, aviation, and other vital industrial industries for high-temperature erosion-resistant applications. Epoxy-filled ceramic microspheres offer remarkable strength and adherence to metallic surfaces, together with good resistance to corrosion and protection against abrasion and erosion. They are employed in marine applications to minimize water tank and ballast erosion. Epoxy resins with ceramic filling are used as coatings on surfaces that are vulnerable to severe corrosion and erosion in chemical process industries. These coatings include hard ceramic particles in the epoxy binders, resulting in ceramic composites with superior mechanical and chemical resistance. These hard ceramic particles in coatings ensure a long life for both the substrate and the coating by rubbing against entrained impurities in fluids without eroding. High-value metal components that have corroded and degraded can also be restored using ceramic metal composites. Engines, gearboxes, bearings, cylinder blocks, liners, casings, flanges, and other degraded components can all be restored through repair. The drawback of ceramic-filled epoxy coatings is the challenge in their application technique. Generally speaking, it cannot be applied using a spray technique. The hardeners and epoxy resins used may be sticky or corrosive to the skin. Therefore, when working with epoxy resins and coatings, nitrile rubber gloves together with barrier cream and cotton beneath gloves need to be worn [16-20].

Polyurethane coatings are often used for effective protection of the aircraft strike areas and leading edges against both gritty particle erosion and rain erosion. Additionally, they are resistant to some de-icing agents and hydraulic fluids containing phosphate ester. The pathways are also coated with specially made polyurethane. Compared to their epoxy equivalents, polyurethane coatings are softer and more elastic, and they are also comparatively durable. Because of this feature, flooring with polyurethane coatings is perfect for moderate to high pedestrian activity. Polyurethane flooring has a slight springiness due to its decreased rigidity, which enables it to withstand severe impact loading. Because of the durability of polyurethane coating, it is also less likely to have dents and scratches, so it is more resistant to abrasion. Because of increased flexibility, polyurethane floors can withstand temperatures below -1°C without losing their mechanical qualities or shape [16-18].

Issues with Using Resistant Materials and Coatings

The use of better materials and coatings for erosion-corrosion control can offer many benefits by extending the service life and reliability of equipment or designed structural components in various industrial settings, improving their performance, and reducing their maintenance and replacement costs. It is, however, seen that the use of such materials and coatings is still far from providing an optimal solution owing to the increasing complexity and cost implications of using optimal materials and coatings, the cost implications of using special equipment, materials, or skills that may be required for the material installations or coating application processes with satisfactory results. The convenience or compatibility and applicability questions of many of the materials in some industrial circumstances, the safety questions of some of the coatings to personnel and the environment, the deterioration or failure inevitabilities of many of the materials or coatings after satisfactory service life in the designed or unforeseeable circumstances [16-22].

From the foregoing, it is apparent that a lot still has to be done in material and coating development to meet various industrial requirements for greater durability and longevity, performance and reliability, versatility, safety level, availability, and affordability at cheaper costs. There is a need to develop smart erosion-corrosion-resistant coatings that can be much more durable and better by their self-repair capabilities than the existing conventional types or build smartness in the existing coating types to enhance their performances [16-22].

Erosion-corrosion Measuring or Testing Devices

Rigs of various, accuracies, advantages, and disadvantages have been developed and used for measuring or testing the effects of erosion-corrosion. Most of the test rigs in existence are the pipe flow loop, jet impingement, slurry pot erosion tester, Coriolis erosion tester, and rotating cylinder apparatus types. In-house devices that are mostly improved versions of the existing devices are also in existence and have continued to emerge [14].

Flow loops are frequently employed in the laboratory for a better understanding of the mechanisms and rates of erosion-corrosion processes under different simulated mechanical and environmental conditions [14]. The ASTM G 76 solid particle erosion-corrosion test standard and the ASTM G 73 high liquid pressure liquid erosion-corrosion test standard cover procedures for conducting the liquid erosion-corrosion tests. Fig. 7 shows a typical test flow loop used for the study of erosion-corrosion behavior around the pipe circle using a designed sensor system. The flow loop consists of a water tank, and a centrifugal pump which is normally used to facilitate the sand particles pass through, a pressure gauge, and a flow meter. According to the measured hydrodynamic parameters, the distributions of the flow velocity, wall shear stress, and sand concentration at certain sections of the pipe shown in Fig. 7 can be evaluated and be well predicted by the Computational fluid dynamics (CFD) simulation. Understanding the non-uniform erosion-corrosion behavior is made simpler by the findings of the CFD simulation. A sample flow loop used to examine the non-uniform erosion-corrosion behavior of an elbow is shown in Fig. 8a. As seen in Fig. 8b, many sensors are positioned at various elbow locations for obtaining localized erosion-corrosion information. As a result, the lack of slurry jet rig systems and rotating disc/cylinder systems for modelling the erosion-corrosion performances of large-scale pipe sections can be adequately addressed by employing test flow loops. However, a rotating disc/cylinder and slurry jet apparatus cannot model the erosion-corrosion behaviors of complicated pipe sections, such as the elbow and pipe weldment, or pipe sections with a change in diameter. The erosion-corrosion behaviors of some typical pipe sections are therefore always studied using test flow loops that enable the installation of various types of sensors. The advantage of the test flow loop is that a more realistic erosion-corrosion state that closely resembles real energy pipelines can be obtained from it. However, because of the pump's wear in the flow loop, frequent restoration or replacement can arise at a significant cost. In terms of attaining real pipe flow conditions, this test setup has the benefit of being extremely similar to industry settings. This rig's shortcomings include its extremely high cost and time commitment, as well as the considerable risk of damage to the pump's propeller after a short usage time. This reduces the reliability of the experimental results due to variations in the flow velocity and actual slurry transfer rate [14].

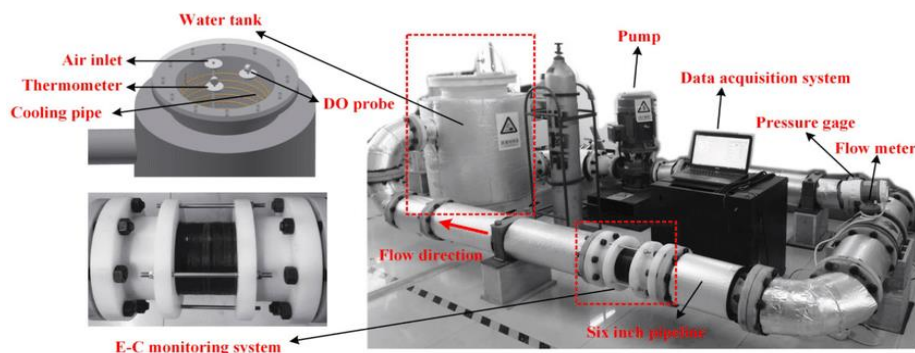


Fig 7: A test flow loop used for the erosion-corrosion behavior around of the pipe circle [14]

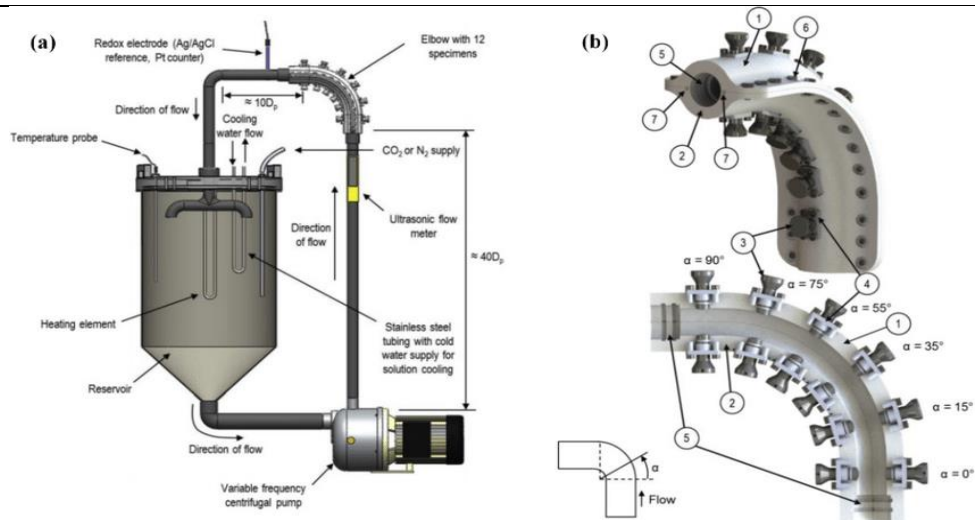


Fig. 8: Schematic diagram of a test flow loop used for the erosion-corrosion study of the elbow (a), and the arrangement of the sensor system at the elbow (b) [14]

The slurry pot erosion-corrosion test device has very simple design. The test device has been in use for over four decades for erosion-corrosion testing of material components. A diagram of the pot tester is shown Fig. 9. The tester usually consists of stainless steel or aluminum cylindrical container, rotating arms, specimen holders, shaft, motor, stirrer and bearings as shown in Fig. 9. The aluminum container is usually of 135 mm height and diameter of 205 mm and is covered with a 12-mm Perspex lid. A propeller is attached at the bottom of the shaft of about 10 mm in diameter to protect against falling solid particles and has uniformly distribute solids in a liquid medium. The test specimens can be 28x6.5x2 mm and are placed in four specimen holders, which are parallel to the central shaft at equal distances. The impingement impact angle ranges from 0 to 90°, but in steps of 15°. The shaft is attached to the motor that drives it. The test specimens are placed on both sides parallel to the central shaft. The flow of the liquid is directed perpendicular to the specimen's axis. In using the tester, an appropriately predetermined mass of abrasive is added to the stainless-steel or aluminum pot, and then tightly closed to fit the lid. After that, an appropriate amount of water is added through the opening in the upper shell to completely fill the pot. The propeller is mounted at the bottom of the pot to maintain the slurry at a distance of 24 mm from the bottom and this part is rotated by a motor. After all testing, the slurry mixture needs to be drained. This test device has advantages and disadvantages. The disadvantages can include the difficulty in controlling the flow conditions and the parameters of the particles, such as the real density of impacting particles and temperature of the slurry. In contrast to the jet type tester, this test device is simple in design, easier to manufacture and use, and very cheap. The bigger advantages of the test device are its ability to be quickly used to conduct simultaneous tests of four coupons of different materials, quickly rank the erosion resistance of different material components, and provide comparatively realistic results for many field applications for the same erosion-corrosion level, relative to most other test rigs [15].

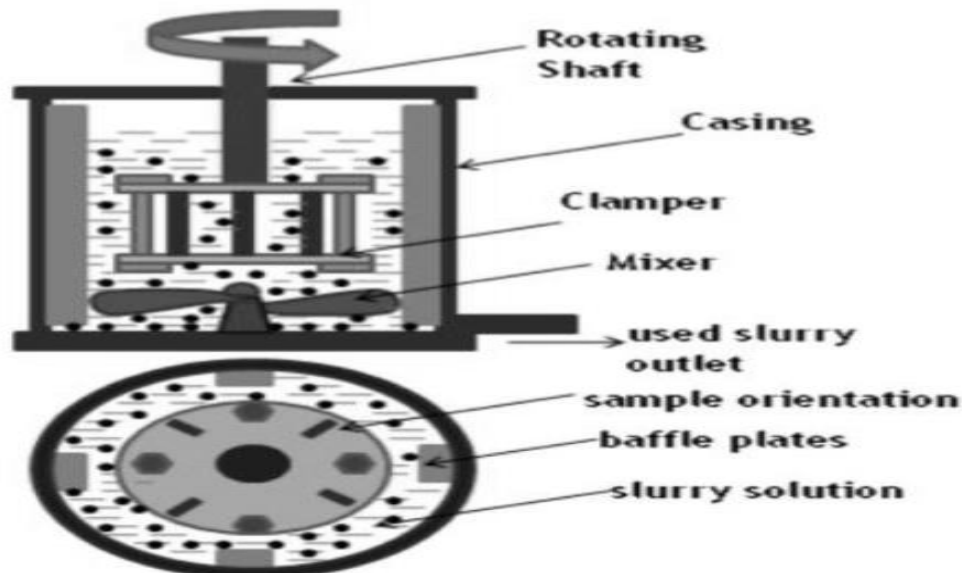


Fig. 9: Slurry pot device used for erosion corrosion testing [15]

Erosion-corrosion tests can also be conducted using a self-made slurry pot erosion apparatus, whose diagram is schematically shown in Figs. 10a and 10b [7]. The apparatus consists mainly of a speed-regulating system, slurry pot accessories, and a temperature controller. A motor with a maximum rotation speed of 1450 rpm drives the stirring impeller to mix the slurry and keep the erodent suspended. The apparatus is equipped with a temperature controller at its top and pipes at the bottom of a water tank, which allow tap water to flow through the water regulating system to maintain the fixed test temperature. The temperatures of the sample and the water are measured using thermocouples. The results are displayed and recorded in real time by the control cabinet with the computer. The specimen holder is fixed to the cover plate. In using the apparatus, the slurry has to be prepared according to the standard requirements with acid and water and poured into the slurry pot. This test device has advantages and disadvantages. The disadvantages may include the difficulty in controlling the flow conditions and the parameters of the particles, such as the real density of impacting particles and temperature of the slurry. In contrast to the jet type, this test device is easier to use, manufacture, and very cheap. A big advantage of this type of test device is the ability to use it to quickly conduct simultaneous tests of four specimens of different materials in comparison to other test rigs with this same erosion intensity.

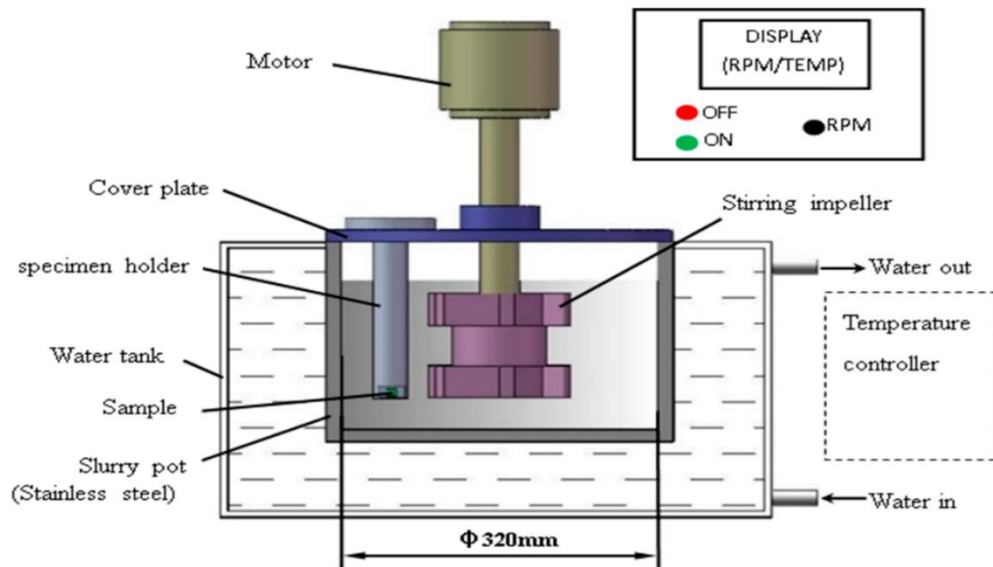


Fig. 10a: A self-made slurry pot erosion apparatus [7]

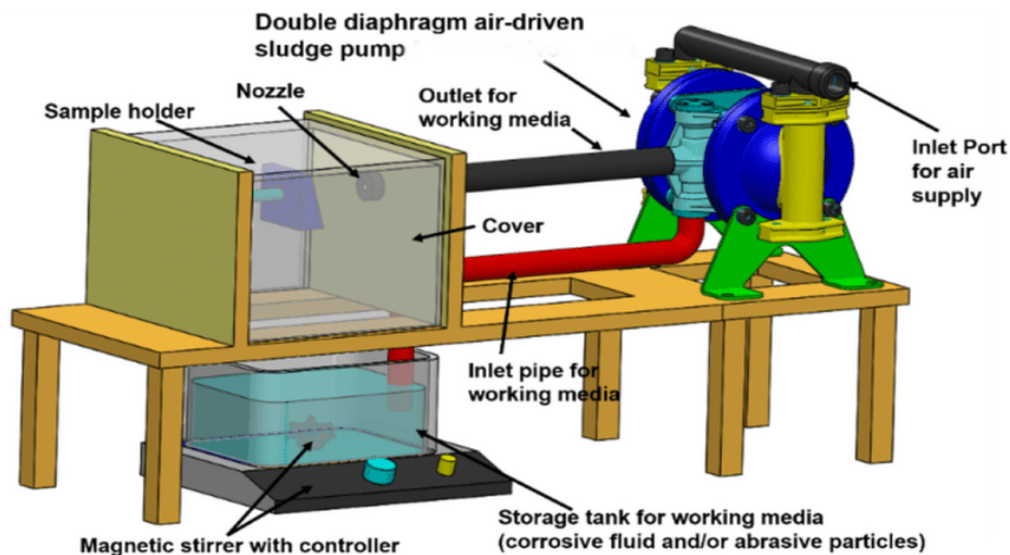


Fig. 10b: Schematic illustrating components of the slurry pot erosion test rig used for experimentation [7]

The Coriolis erosion tester has been developed since 1984 for investigating the movement of slurries and their interaction with surfaces such as pumps and pipelines [15]. The current version of the tester uses flat test specimens of dimensions of 29 x 15 x 6 mm. The scheme of the tester is shown in Fig. 11a and Fig.11b. The tester uses centrifugal and Coriolis forces. Freshly prepared slurry from the container is fed into the center of the rotor of diameter 150 mm, where there is a slurry inlet port of diameter 12.7 mm. The specimen holders are located equidistant from the center of rotation of the rotor. In the specimen holders are the

channels through which flows the slurry, while the base of the channel forms the specimen that is under test. The channels are about 1 mm wide and 6.35 mm high with a rectangular cross-section. The specimen under test rotates at a speed up to 7000 rpm. The tester uses a 1.5-kW electric motor and speed controller under low impact angle. Slurry is accelerated outwards by centrifugal force, while under the influence of Coriolis force, erodent particles settle on the surface of the test specimen, thereby increasing the interaction of the slurry with the surface of the specimen. Due to high rotation speed, this method shortens the testing time. The design of the tester allows simultaneous testing of two specimens. The advantages of this test rig include its ease of use, speed, and superior control over experimental conditions. It is good for ranking the erosion-corrosion resistance of slurry pump components and replicating the action of slurries moving inside centrifugal pumps and cyclones. However, it is only appropriate for flat test specimens and only replicates erosion under low contact intensity at low impingement angles and velocities.

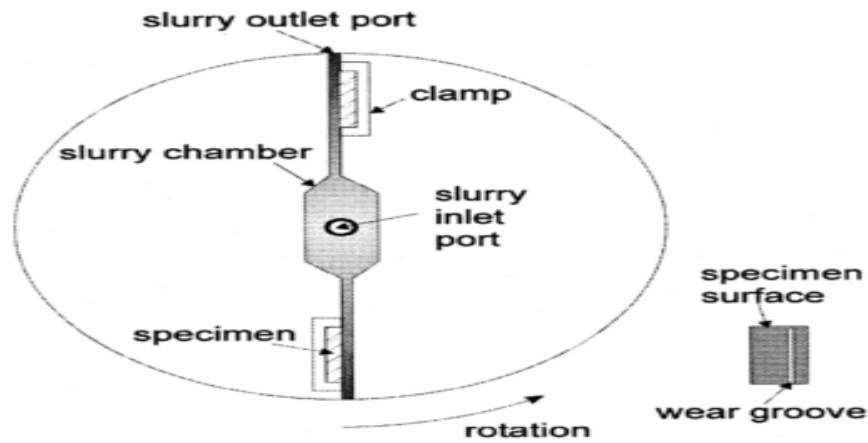


Fig. 11a: Top view of the Coriolis erosion corrosion tester [15]

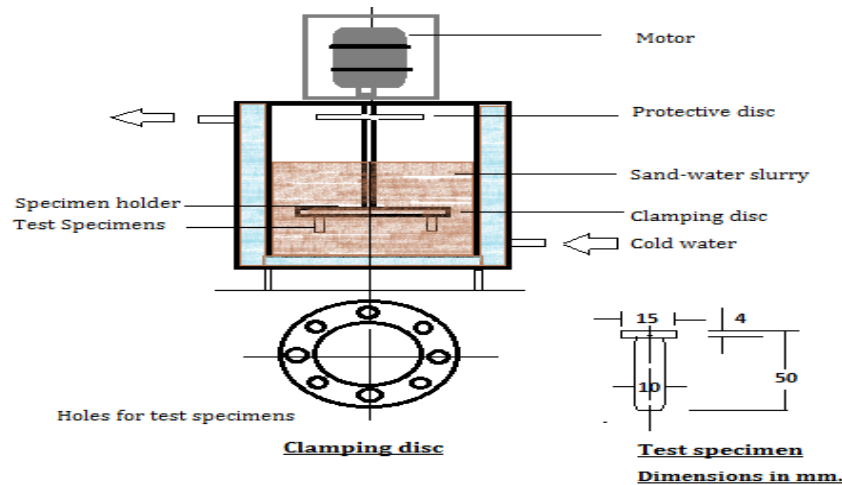


Fig. 16. Side view of the slurry erosion test set-up [11b]

Xu et al. [11, 13] demonstrated that a convenient way to simulate an erosion-corrosion environment is through a rotating disc/cylinder arrangement. Due to its comparatively low cost and simple operation, the rotating disc/cylinder electrode system has been extensively utilized in the flow-accelerated corrosion (FAC) and erosion-corrosion investigations since 1950. The revolving disc/cylinder systems used in erosion-corrosion experiments can be seen in two different configurations shown in Fig. 12. Both test sets consist of a rotating disc or cylinder to replicate a hydrodynamic condition and a three-electrode system. The test sample itself functions as the spinning cylinder in the first set, as illustrated in Fig. 12a, whereas the test specimen in the second set is positioned at the edge of the rotating disc. In the first set, the rotating speed can be used to easily regulate the linear velocity on the sample surface. The steel sample submerged in the first set develops a more uniform corrosion pattern than in the second set. All of the metal loss from erosion in the first set comes from the tangential direction at the beginning of the test because the angle between the sample and the flow direction is constant. In the second set, however, the angle between the specimen and the flow direction can be changed from 0° to 90° [11,13].

The rotating disc/cylinder technique, however, has several flaws, which prevent it from being used in many situations. The management of the sand content when corrosive slurry is put into the test cell is the most problematic aspect of the rotating disc/cylinder electrode system. The distribution of the sand in the test cell is not uniform; therefore, even though the overall weight percentage or volume percentage of the sand particles in the entire test cell remain the same, the actual sand concentration

at various liquid levels would be very different [11, 13]. The real sand concentration at the corresponding liquid level would change with variations in rotation speed since the samples are fixed at a specific height. The evaluation of the sand concentration's impact on the erosion-corrosion behavior is restricted by the uncontrollable sand concentration. However, it is impossible to analyze the erosion-corrosion performance under a single-particle impact due to the rotating disc or cylinder's design. In the test cell, the erosion-corrosion environment is purified as a pure electrolyte or slurry. The sand particles in the test cell cannot be replaced when the sharp edges of the sand particles are smoothed after extensive erosion, as the rotating disc/cylinder test cell is a wholly sealed system. The erosion-corrosion strength could be weakened by changing the form of the sand [11, 13].

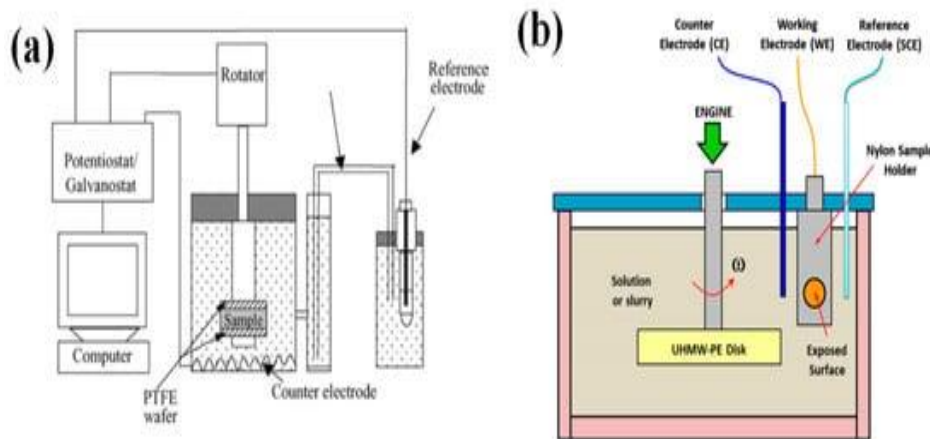


Fig. 12. Typical rotating disc/cylinder electrode systems used for erosion-corrosion (a) with the electrode acting as the rotating cylinder and (b) with the electrode being arranged at the edge of the disc [11]

A jet type apparatus is a different form of device that can be used for erosion-corrosion testing [15]. According to the name of this device, the slurry, liquid with solid particles as a jet impacts the target material component, which may be stationary or rotating. In rigs with rotating specimens, a specimen crosses a slurry jet, causing cyclic collisions. In case of devices with a stationary specimen, a specimen is continuously exposed to a slurry jet. The device, in which a test specimen is fixed to a rotating arm or disk, is described in the ASTM G-73 standard. The whirling specimen crosses a jet with frequency depending on velocity of rotating disk as showcased in Fig. 13. The jet velocity is in the range of 50 to 1000 m/s, and the nozzle diameter ranges from 0.1 to 5 mm. Slurry is pumped through the impeller system and directed at the specimen via a nozzle. There is therefore a risk of pump damage because the solid particles impact the rotor blades with different velocities, which can lead to faster pump wear. The test devices are based on ASTM G 73 Standard. The rig is convenient and reproducible, and facilitates easy control of impingement angle and velocity. The main disadvantage of this device is the impact velocity and impact angle of all the solid particles do not remain the same during the test..

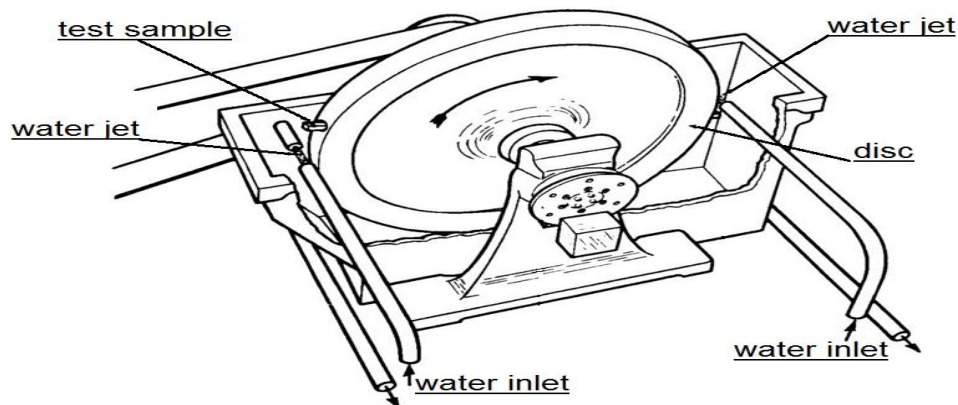


Fig. 13: Rotating disk and jet repetitive impact apparatus, according to ASTM G 73 [15]

A jet-type test rig shown in Fig. 14 was created in-house for slurry erosion testing [23]. The test rig belongs to the non-recirculating kind, in which sand particles are not reused after passing through the system just once. This aids in a more accurate representation of the working environment. Fig. 14 displays the test rig's organized design. This apparatus allows for independent control of the abrasive particle concentration, size, impact angle, and velocity of the specimen in relation to the jet of slurry. By adding a known quantity of sand to the mixer seen in Fig. 14, the concentration of the slurry is managed. By counting the quantity of sand exiting the nozzle, the sand concentration is calibrated. To reduce the variance in nozzle diameter during experiments, a

tungsten carbide insert is used to create a nozzle with a 4 mm diameter. Additionally, throughout the experiment, the nozzle's exit diameter needs to be measured repeatedly to look for any changes. An ultrasonic flow meter is used to continually measure the slurry's flow and velocity during the experiment. The meter is calibrated by counting the amount of water that is discharged from the nozzle using the discharge method [23].

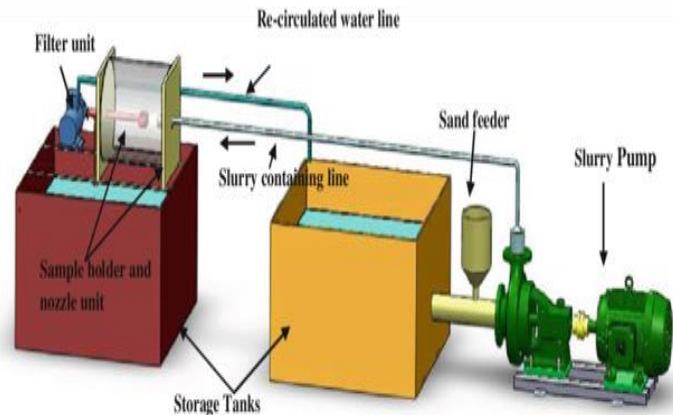


Fig. 14: A created in-house jet-type test rig employed for slurry erosion-corrosion testing [23]

A designed and produced jet-type erosion-corrosion test rig whose setup is depicted in Fig. 15 is another form of slurry erosion test rig that can be used to carry out tests. With the use of the test rig, experiment factors including the impingement angle, sand concentration, working medium, and impact velocity may be controlled with flexibility [24]. By altering the frequency of the motor converter operating the pump, the velocity of the slurry jet can be adjusted. The drive motor's rotation speed can be changed to alter the sand concentration. For slurry erosion studies, irregular sand particles in the size range of 16-40 mesh are utilized. Slurry is created using sand in quantities of 10 kg/m³ and 30 kg/m³. With a 5-minute cycle, each sample can be evaluated for 30 minutes. The specimen and the ejector nozzle are usually spaced 6 cm apart in each investigation. The eroded samples are properly cleaned using an industrial acetone solution to get rid of impurities, then dried. The mass loss of the samples is measured at regular intervals before and after the test using a precision balance with a 0.1 mg accuracy level. The erosive wear rate is calculated based on the cumulative mass loss of the sample with time, that is, mg/min. The eroded surface characterization can be examined by the scanning electron microscope (SEM) [24].

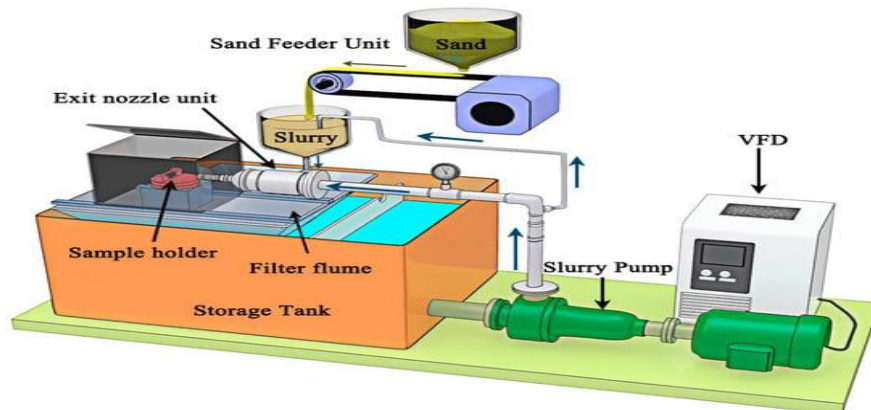


Fig. 15. Schematic view of the slurry erosion test rig [24]

Slurry erosion-corrosion and slurry erosion tests can also be carried out using a designed slurry whirling arm rig, shown schematically in Fig.16 [25]. The erosion tester is designed to control and adjust impact angle, particle impact velocity, and particle concentration. The tester is composed of a slurry unit which acts as a reservoir tank and allows mixing of solid particles in the slurry, a vacuum unit which eliminates aerodynamic effects on the slurry system, and a specimen rotation unit. In the whirling test rig, the wear specimens are rotated in a vacuum chamber and a jet of solid liquid falls on the specimen due to gravity flow. The rig is composed of a specimen rotation unit, a slurry unit, a vacuum unit, and other parts as shown in Fig.16. In this test rig type, two specimens are clamped in specimen fixtures mounted on two horizontal arms rotated by a variable speed electric motor. The effective rotation diameter of the whirling arms is 248 mm. The specimen fixtures have tilting and locking facilities to adjust the required inclination of the test specimen. The specimen rotation unit provides impact velocity. During slurry erosion tests, only the front surface of specimen is exposed to the impinging slurry since the other sides of the specimen are held by the specimen fixture. The front surfaces of the specimens, test surfaces should be 23mm × 10 mm. The impact angle can be adjusted to any required value by rotating the specimen holder around its horizontal axis, as shown in Fig. 16. This assembly is kept in a

vacuum chamber as shown in Fig. 16. The slurry in the chamber falls freely under gravity from a barrel of 25-liter capacity, where a stirrer is used to keep the solid-liquid under suspension. The erosion-corrosion tests are carried out in corrosive slurry containing 1% weight of silica sand and 3% weight of NaCl aqueous solution. For comparison, slurry erosion tests are conducted under the same particle concentration free from NaCl and the weight loss rate in the water slurry is referred to as erosion rate. The test specimens are cleaned in acetone and then weighed for weight loss using electric balance with an accuracy of 0.1 mg. The velocity of falling slurry stream from the 3 mm diameter funnel orifice is designed to be 1.67 m/s, at the specimen surface, impacting every specimen at any pre-set angle between 0 and 90°. The impact angle (θ), and impact velocity (v) are correlated to ensure the intended value, which can be obtained from the velocity vector diagram of particle impact, as shown in Fig. 13. The impact velocity of slurry stream can be from 15 m/s. The distance between the funnel orifice and the specimen surface is 40 mm. The slurry test chamber is evacuated by a vacuum system of up to 28 cm Hg to minimize aerodynamic effects on slurry system [25].

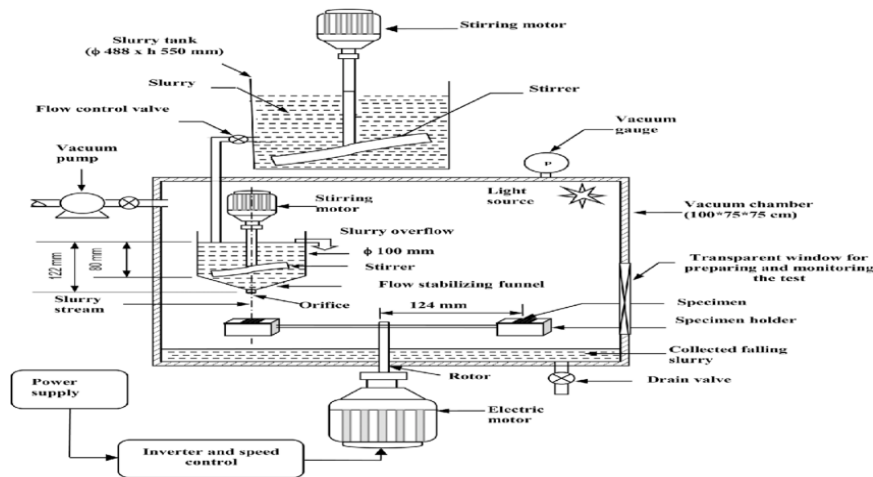


Fig. 16: An erosion-corrosion test device [25].

Another method of conducting erosion-corrosion test is by using electrochemical devices and coupons in test set shown schematically in Fig.17 [26]. The flow condition in the cylinder test cell is generated by a rotating disc. The detailed specifications of the device include the disc diameter of 60 mm, disc thickness 20 mm, and the test cell inner diameter 80 mm. A coupon electrode and a wire beam electrode (WBE) is installed in the test cell through the remained holes on the cell wall. The margins between the samples and the cell wall are sealable by silicon glue. The center of the coupon electrodes and WBE needs to be flushed with the disc center. The side length of the coupon electrode is 7 mm. The coupon electrode should be connected to an Ag/AgCl reference electrode and a titanium mesh counter electrode is to be used to construct a three-electrode system using an electrochemical workstation (Reference 600+, Gamry, US). The WBE is fabricated with 100 tiny square electrodes of side length 2 mm. The interval of the tiny electrodes is 0.2 mm. The WBE is connected to a multiplexer (YC-2200A, Yun Chi, China) containing 10 channel zero resistance meters. Both the coupon electrode and the WBE are made of the test material such as the X65 steel for the case shown in Fig. 17, The surfaces of coupon electrode and the WBE should be gradually polished from about 400 to 1200 grit papers before the test, to ensure that the initial working surface condition of both the coupon electrode and the WBE remain the same. The composition, microstructure, surface hardness, yield strength, and ultimate tensile strength of the coupon material need to be specified for better analysis of the test results and understanding of effects of the erosion-corrosion [26].

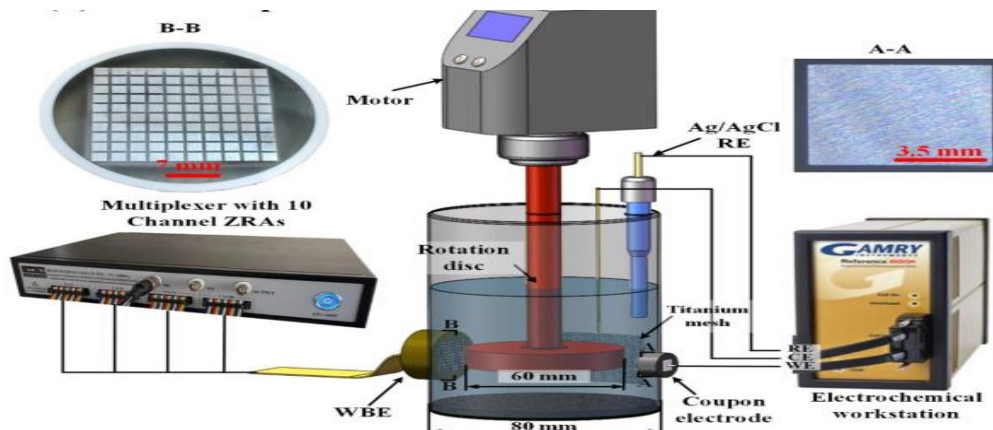


Fig. 17: schematic diagram of erosion-corrosion test setup using electrochemical devices and coupons [26]

Erosion-corrosion tests can also be carried out utilizing a whirling arm slurry erosion test rig (WASET) shown in Figs. 18a and Fig. 18b [27]. The rig is made up of three primary components; a vacuum unit, a slurry test chamber, and a slurry mixing unit. 1% sand particles are added to tap water and stirred with a stirrer in a 25-litre cylindrical tank before introducing it to the slurry mixing device, where the resulting slurry is then piped into the slurry test chamber. The slurry mixture is introduced into the slurry test chamber using a funnel with an aperture of diameter 3 mm and a stirrer to maintain the slurry's suspension. At the center of the sample surface, the funnel creates a stream of homogenous, stable slurry that continuously drops. To balance the dynamic forces, test specimens are put on two holders that are attached to the ends of two horizontal arms that are spaced 180 degrees apart. Samples are placed 40 mm from the orifice's tip, with a diametric holder-to-holder distance of 248 mm. As seen in Fig. 18b, the sample holder can be turned around the arm axis to change the impact angle from 0° to 90°. The two arms are fastened to a brass sleeve that is tightly fastened to the top of a vertical whirling shaft that is powered by a variable-speed motor and provide balance during high-speed operation. A single surface measuring 23 mm by 10 mm for each of the two samples under test is exposed to the slurry stream at impact angles of 30°, 45°, 60°, and 90°. The slurry test chamber is evacuated by a vacuum system up to a pressure of 28 cm Hg to remove aerodynamic influences on the slurry stream. The same approach is used for the second set of studies (erosion-corrosion tests), but samples are subjected to a slurry including seawater (tap water +3.5% NaCl) rather than tap water. Predetermined amounts of pure water (or seawater) and SiO₂ sand flow are mixed continuously in the slurry tank to replace the used slurry during any set of experiments. A precision scale with an accuracy of 0.1 mg is used to precisely weigh the specimen before and after each of the measurement periods that are performed for each test condition [27]

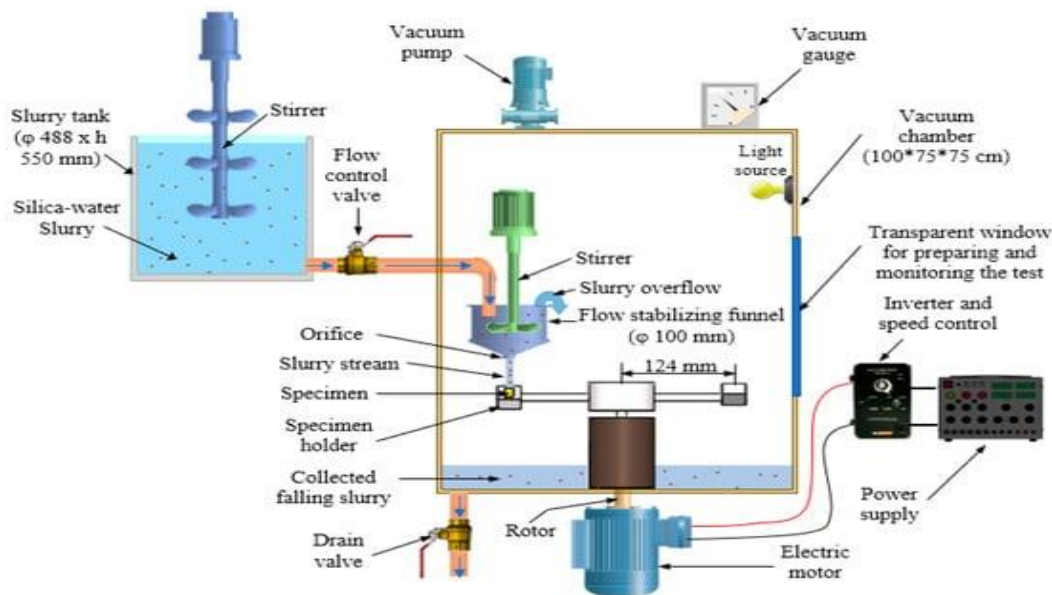


Fig. 18a. Schematic view of the slurry whirling-arm rig [27].

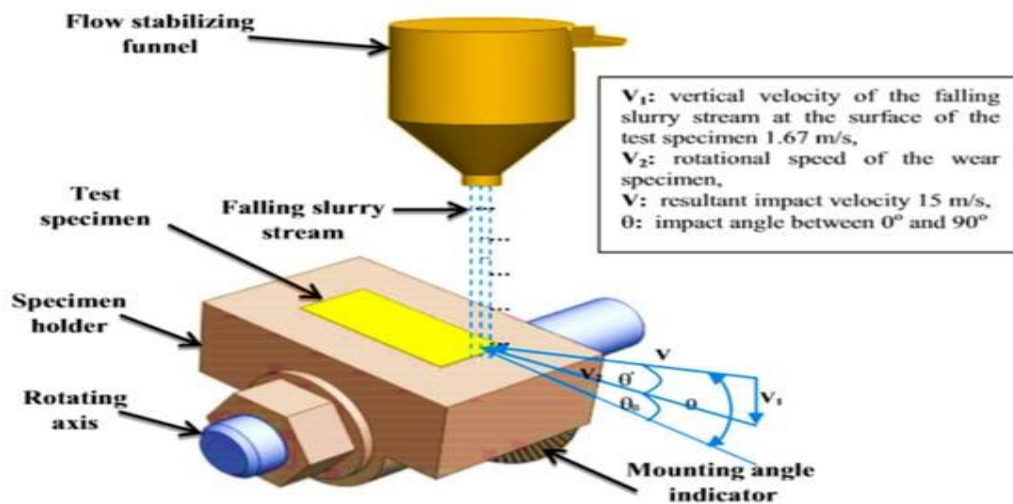


Fig. 18b: Schematic diagram of the impact angle and impact velocity [27].

Another type of set-up used for erosion-corrosion test is shown in Fig. 19 [9].

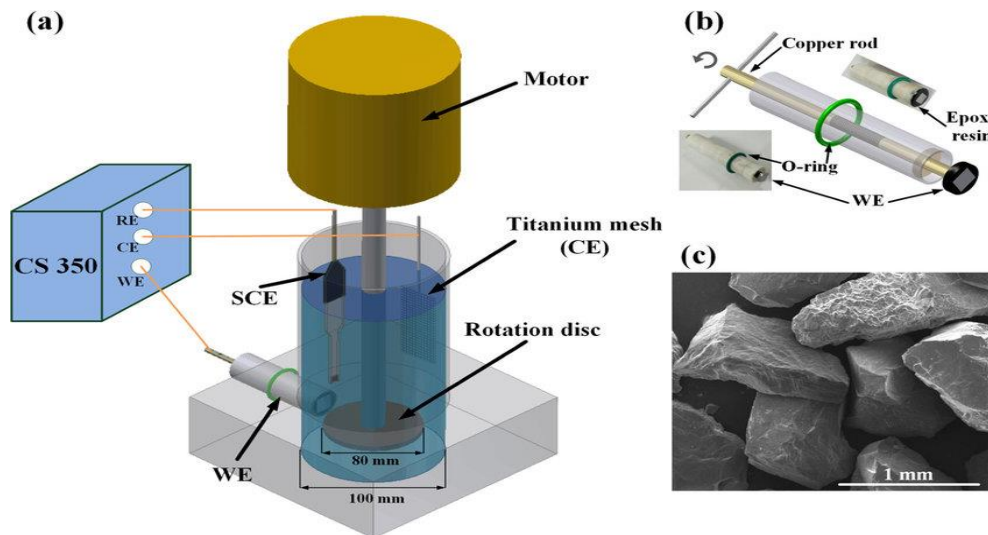


Fig. 19: The erosion-corrosion test setup (a)The rotation disc system. (b)The structure of the sample holder. (c)The SEM image of the silica sand particle [7, 9]

The set-up in Fig. 19 consists of a stirring system and a glassy test cell. The rotation disc is made of Teflon with a diameter of 80 mm and a thickness of 10 mm. The rotation speed can be adjusted from 0 to 3000 rpm (100 rpm step) using a motor. A specially designed Teflon sample holder is used to install the working electrode (WE), as shown in Fig. 19b. The WE are made by sticking a copper rod to the steel electrode from the back side using conductive copper tape and then sealing with an epoxy resin for electrochemical measurement. The gap between the sample holder and the glassy cell is sealable using an O-ring. After the test, the copper rod and the WE are separable by rotating the screw on the copper rod as shown in Fig.19b. Then, the WE are peelable from the epoxy resin by heating the sample to 250 °C. Consequently, the weight loss of the WE are measured after acid cleaning. The exposed surface of the WE are 7 mm × 7 mm. All the electrodes are made of X65 pipeline steel with the chemical composition by percentage weight of; 0.04% C, 0.2% Si, 1.5% Mn, 0.011% P, 0.003% S, 0.02% Mo, and Fe the balance. The microstructure of the X65 pipeline steel is composed of uniformly distributed ferrite and pearlite [7, 9]. The surfaces of the WEs should be polished using SiC papers of 600 down to 1000 grit, followed by washing with ethanol and distilled water and finally drying in hot air. The WE should be mounted close to the cell wall as shown in Fig. 19a. The distance between the WE and the edge of the rotation disc should be about 9 mm. The center of the WE are placed at the same level of the rotation disc. The distance between the rotation disc and the bottom of the cell should be 5 mm. A titanium mesh should be used as the counter electrode (CE) and a saturated calomel electrode (SCE) be used as the reference electrode (RE). The electrodes are connected to a CS 350 electrochemical station for EIS and PDP measurements. The 3.5 wt.% NaCl solution entraining 10 wt.% silica sand particles was used as the test slurry. The average diameter of the sand particles is 1 ± 0.2 mm, and the particles have irregular shapes with some sharp edges as shown in Fig. 19c. Nine rotation speeds of 0, 100, 200, 300, 500, 1000, 1500, 2000, and 3000 rpm were selected to study the corrosion and erosion-corrosion behaviors under different flow rates. During the test, the solution was directly exposed to the air to ensure sufficient dissolved oxygen in the slurry. The test cell was placed in a temperature controller which provides a continuous flow of air to cool down the cell. The pH of the solution was 6.7, and the fluid temperature slightly increased from 29 to 36 °C with increasing the rotation speed from 100 to 3000 rpm. The changes in pH before and after the EIS tests were less than 0.1 for all cases. The concentration of the dissolved oxygen slightly decreased from 6.6 mg/L at static speed and 29 °C, to 6.2 mg/L at 3000 rpm and 36 °C, due to the temperature increment. The Reynolds number (Re) in the test cell can be calculated as in Eq. 10 [9]:

$$Re = \frac{\omega r^2}{\nu} \dots \dots \dots (10)$$

Where ω is the rotation speed, r is the radius of the rotate disc and ν is the kinematic viscosity of the electrolyte. It is calculated that the Re ranges from 2.3×10^4 (100 rpm) to 6.9×10^5 (3000 rpm) at different flow conditions, suggesting completely turbulence flows in the cell. EIS measurements in conjunction with gravimetric measurements were performed, aiming to investigate both corrosion metal loss and total metal loss under different flow rates. EIS measurements were conducted every 2h with a 10-mV sinusoidal signal over a frequency range from 105 to 10⁻² Hz around OCP. The EIS measurement results were then fitted. by Z View. After 24 h of the test, the steel surface was cleaned using ASTM G1-03 solution. A high-definition digital camera was then used to take images from the corroded surfaces. The surface morphologies of the WEs at some typical flow conditions were further observed by a scanning electron microscope (SEM) type, FEI Quanta 200. The local 3D profiles of the WEs were scanned by an Olympus infinite microscope. After the elimination of the epoxy resin,

the weight losses of the WEs can be measured using a Shimadzu A UW 320 balance scale with an accuracy of ± 0.1 mg. The test as conducted under each rotation speed can be repeated three times to ensure the repeatability of results. PDP measurements need to be performed to investigate the propagation of the electrochemical reaction under different rotation speeds. As PDP measurement would take a longer time and the strong polarization can significantly influence the erosion-corrosion process, the PDP measurements can only be conducted within few hours such as 4 to 20 hours at each rotation speed [7, 9].

Fresh WEs are used for each polarization measurement. In the static electrolyte, the WEs are polarizable from -300 (vs. OCP) to 0 mV (vs. SCE) with an anodic scan rate of 1 mV/s. In the flowing slurry, the WEs are polarizable from -350 (vs. OCP) to 350 mV (vs. OCP) with an anodic scan rate of 1 mV/s. Each polarization curve can be measured twice to ensure the repeatability. Since the erosion-corrosion performances of the steels under some rotation speeds can be similar, parts of the measurement results and surface morphologies obtained under 100 , 500 , and 2000 rpm should also be provided. [7, 9]

A cylindrical stirring electrolytic cell showcased in Fig. 20 is another equipment type employed for erosion-corrosion tests [28].

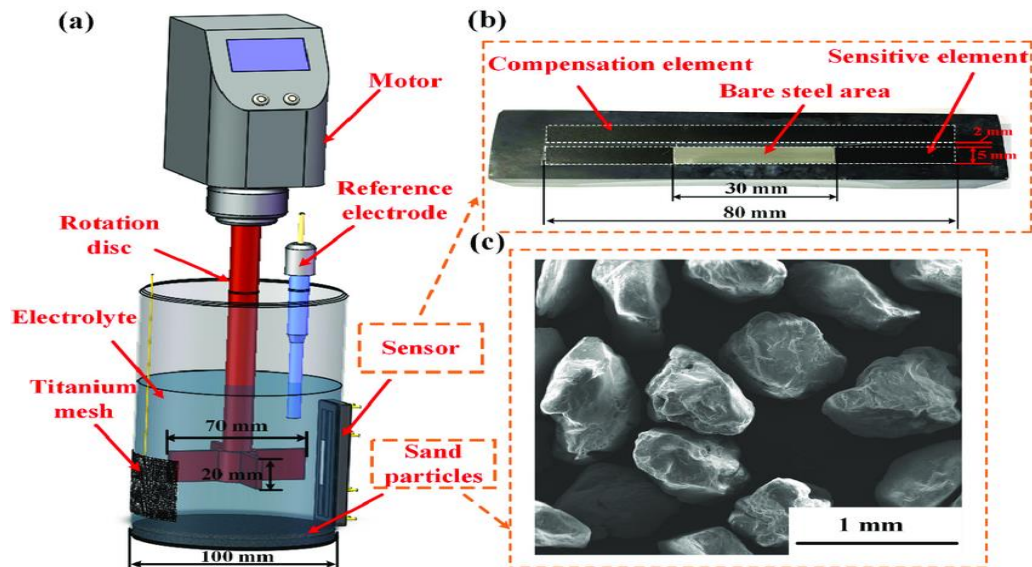


Fig. 20. The test setup for erosion-corrosion showing (a) schematic illustration of the cylindrical stirring electrolytic cell, (b) photo of the erosion-corrosion sensor and (c) SEM image of the sand articles [28].

The diameter and height of the test cell are 100 mm and 200 mm, respectively. A four-blade propeller is used to stir the solution with a diameter of 70 mm and a thickness of 20 mm. The distance between the bottom of the electrolytic cell and the propeller is 30 mm. The rotation speed of the propeller is adjustable from 0 - 3000 rpm through a frequency conversion motor. A detailed schematic representation of the erosion-corrosion sensor is shown in Fig. 20b. When conducting erosion-corrosion experiment, the erosion-corrosion sensor can be fixed on the wall of the electrolytic cell with the bare steel area at the same height as the propeller. The surface of the bare steel area is flushable with the wall of the cell. The gap between the erosion-corrosion sensor and the wall of the cell can be sealed by hot melt glue. The sensitive element and the temperature compensation element are both made of X65 pipeline steel, with chemical compositions by percentages mass of 0.12 C, 1.27 Mn, 0.18 Si, 0.008 P, 0.002 S, 0.17 Mo, 0.11 Cr, 0.12 Cu, 0.07 Ni, 0.022 Al and Fe the balance. Copper wires are soldered on the back sides of the electrodes using copper foil tape to keep electrical connection with the resistance meter and the electrochemical workstation. The surfaces of the sensitive element and the temperature compensation element are successively grounded using 400 – 1000 abrasive papers before the tests. The polished surfaces are then washed with acetone and rinsed with distilled water. An Ag/AgCl electrode and a titanium mesh are used as RE and CE, respectively. The 3.5% NaCl solution entraining 10% silica sand particles by weight is used as test medium. The shape of the sand particles is shown in Fig. 20c, with an average diameter of 600 μm [28].

Erosion-corrosion tests can be conducted under four rotation speeds of 200 , 500 , 1000 , and 2000 rpm. At each rotation speed, varied current densities of 1 , 2 , 3 , 4 , 5 , and 6 milliamperes per square centimeter are sequentially applied on the surface of the sensitive element, with each applied current lasting for two hours. The erosion-corrosion rates of the sensitive and compensation elements are measured every 10 min. After the erosion-corrosion tests, the sensitive elements are immediately taken out of the cylindrical stirring electrolytic cell and cleaned by the pickling agent suggested in ASTM G1-03 standard cleaning procedure. The depth profiles and the local 3D profiles of the steel surface are observable with an ordinary least square (OLS) 5000 infinite microscope (Olympus, Tokyo, Japan). Moreover, the local morphologies of the surface of the sensitive element can further be observed using a scanning electron microscope (SEM). The erosion-corrosion test should be repeated three times at each rotation speed to ensure the repeatability of the results. In addition, the polarization curves of the sensitive element are measured at each rotation speed with a scanning rate of one millivolt per second (mV/s), which should be used to calculate the compensated cathodic current of the sensitive element [28].

Erosion–corrosion tests can also be conducted using the test rig shown in Fig. [29] [22].

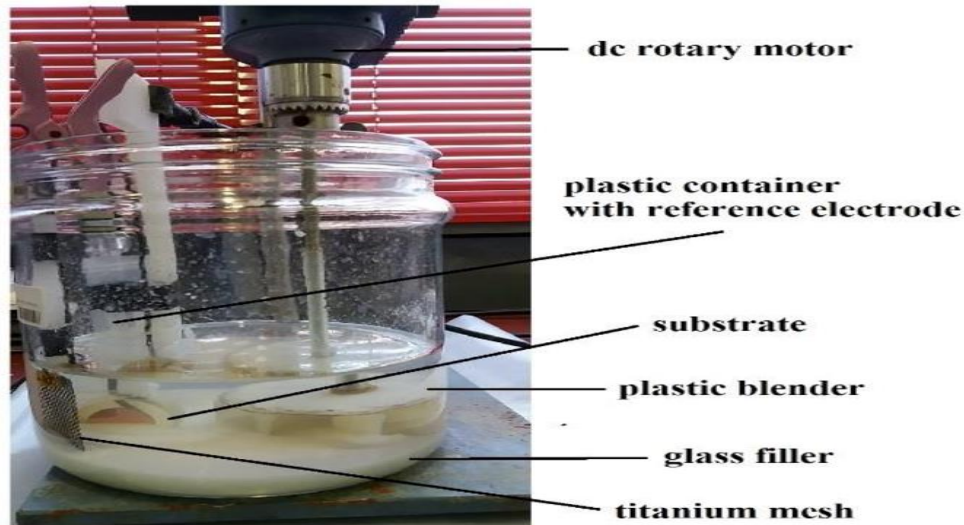


Fig. 21. A test rig used for erosion–corrosion experiments [29]

The setup consists of a glass beaker including one-liter solution. In particular, the solution slurry is obtained by mixing 3.5% NaCl with 40% glass grinding filler (average diameter 200–300 μm) by weights. A DC rotary motor should be connected to a plastic blender, which throws the sand particles with a constant rotational speed of about 500 rpm at the sample surface. On-site electrochemical impedance spectroscopy (EIS) can be performed using a three-electrode configuration (coated sample as working electrode, Ag/AgCl probe as reference electrode, activated titanium mesh as a counter electrode). For the purpose of determining the water contact angle (WCA) of the samples after each cycle of erosion-corrosion, they should be removed from slurry solution, washed with deionized water, dried, and rested for two weeks in open to air conditions [29].

Jet impingement is usable for flow corrosion testing due to the hydrodynamic characteristics of a jet impinging on a flat plate. The fluid flow across the flat surface contains characteristic flow regions that are mathematically definable. Placing the working electrode of the test probe at a specific radial location in the jet allows measurement of the corrosion rate under those specific conditions. A jet impingement test apparatus that is simpler and easier to operate than previous existing designs and provide vastly superior temperature control without the temperature fluctuations that occurs with immersion heaters was developed by Daniel Efir [30]. A schematic diagram of his jet impingement test cell, showing the relative position of the jet, test probe, and thermocouple monitoring the fluid temperature inside the cell, is shown in Fig. 22. The wall shear stress range obtainable with this system is from 20 to 1000 Pa. Modification of the basic re-circulating liquid apparatus allow flow-through operation and/or operation with liquid containing entrained gas, simulating multiphase production and gas lift systems. The jet impingement test system is combined with corrosion probe technology, allowing linear polarization corrosion measurements in high resistivity systems. This permits the application of jet impingement techniques to gas flow with entrained liquid simulating annular flow conditions in gas production systems and to oil flow with entrained water phase simulating low water cut multiphase production [30].

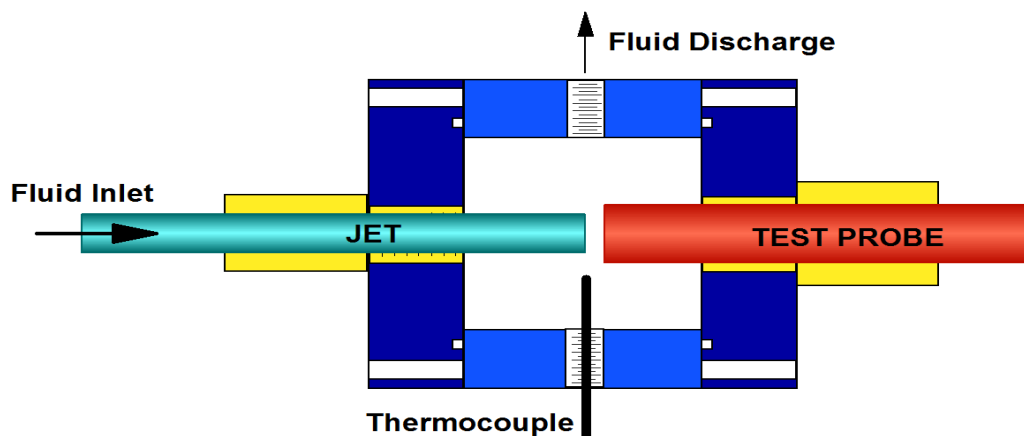


Fig. 22: Schematic diagram of the jet impingement apparatus test cell [30].

Slurry erosion testing can also be conducted using a specially designed test rig shown in Fig. 23 [31]. This test rig facilitates testing materials at different sets of parameters. The rig has built-ins by which impact velocity (v), mass flux rate (m), the angle of impingement (h), particle size (S), distribution (d), and standoff distance between the nozzle outlet and target surface can be individually controlled. The rig originates from a design known as the non-recirculation type, which mimics the actual working environment of the fluid equipment, especially pumps and turbines. Slurry erosion testing is conducted with the rig in accordance with the ASTM G-73 standard procedure. Coupons are cut into sizes measuring 10 mm diameter and 10 mm thick using wire-cut electro-discharge machining (EDM). The roughly finished surfaces of the coupons are polished with 2500-grit emery paper. Before testing, all the coupons, coated and uncoated, should be ground using emery paper down to 1500 grit size. Thereafter, they should be polished using 1 μm alumina slurry paste on a disc polishing machine. Mass loss measurements are performed using a precision analytical balance with the accuracy capability of measuring up to 0.0001 mg. After the test, initially, there can be an increase in weight due to the addition of corrosion products. Hence, to remove the products, the coupons should be washed with water and concentrated HCl acid solution combined in the ratio of 2:1, respectively, and dried in air before weight measurements. Natural silica sand sieved to a nominal size range of 50–344 μm is usually used as an erodent. The average silica sand prior to the test is in a size range of 220–500 μm . It is noted that the size of the sand particles gets reduced from the nominal size range of 344–177 μm . The rate of erosion-corrosion test using this rig is calculated from Eq. 11.

$$CR = \frac{KW}{ATD} \dots \dots \dots (11)$$

The corrosion rate is measured in mm per year (mm/yr), $K = \text{Constant } (8.76 \times 10^4)$, $T = \text{time of exposure in hours}$, $A = \text{exposure area in cm}^2$, $W = \text{mass loss in grams}$, and $D = \text{density in g cm}^{-3} (8.94 \text{ g cm}^{-3})$

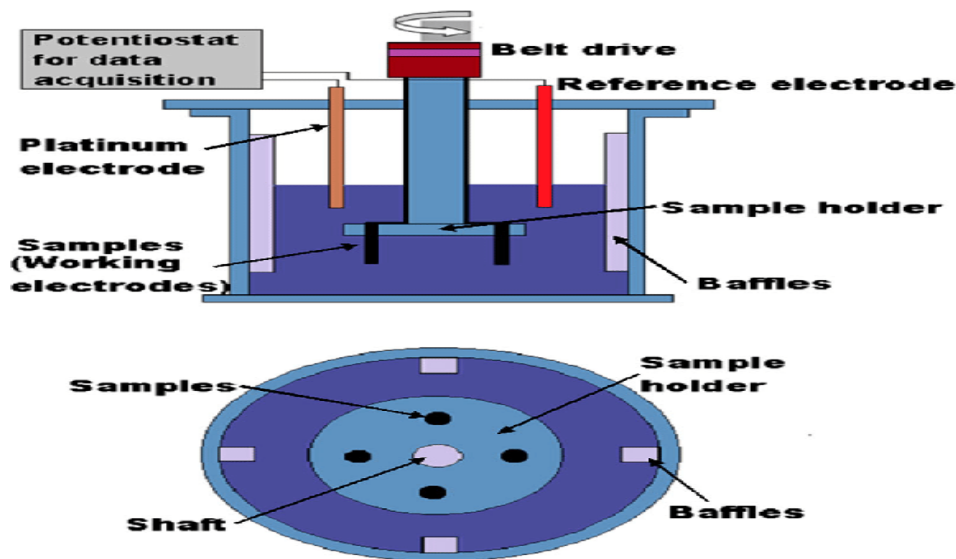


Fig. 24: Schematic of an erosion-corrosion test rig [24]

Some Research Woks on Erosion-Corrosion

IV. Research works based on Conventional methods

Some of the research works on erosion-corrosion using the traditional methods are outlined in this section.

Azhari *et al.* [3] investigated the effect of waterjet treatment on the surface characteristics of carbon steel 1045. In particular, they investigated the effect of waterjet treatment parameters, namely the number of jet passes and pressure. They found that an increase in the number of jet passes as well as pressure led to higher roughness and more erosion of the surface. They also found that the damage features consist of various fracture mechanism modes at the initial and evolved damage stages. They reported that the ferrite phase experienced more damage than the pearlite phase. They, however, observed that the damage was more concentrated along the grain boundaries. They observed that the shearing force from the jet lateral flow raised the circumferential rim and created lateral cracks and sub-tunnels, which might eventually be removed in the subsequent jet passes. They finally reported that the hardness of the treated specimens increased with an increase in the number of jet passes and pressure.

El-Midany *et al.* [5] devised and built a test apparatus to facilitate testing material specimen resistances to slurry erosion and cavitation erosion. The apparatus was tested by submerging the specimens in a tank filled with slurry that had the appropriate fluid composition and concentration. The specimen was then allowed to rotate using the holder shaft at a predetermined speed, ranging from zero to 900 rpm. They found that cavitation causes erosion when a specimen with a cross section like a pipe or an aero foil section rotates at a fast rate in a fluid. The velocity and the cross-sectional profile of the specimen determine the

pressure. The rotation of the specimen holder, N (rpm), and the radius from the specimen's center of rotation around the axis (r) can be adjusted to regulate the relative velocity between the specimen and slurry. Eq. 12 gives the relative velocity (v).

$$v = \omega r \dots \dots \dots (12)$$

Where ω is the angular velocity of the specimen holder and is given by Eq. 13

$$\omega = \frac{2\pi N}{60} \dots \dots \dots (13)$$

According to Zadeh [10], practically any component that comes into contact with corrosive fluid is susceptible to corrosive erosion. In the meantime, the erosion-corrosion phenomenon severely affects heat exchange systems, transmission lines of corrosion fluid in industrial reactors, as well as gas, oil, and water transmission pipes. Because of their interaction, erosion-corrosion can result in material loss that is significantly greater than the total of pure erosion and pure corrosion alone. The two main modes of erosion-corrosion in aquatic systems are mechanical erosion and electrochemical corrosion. On account of the greater material loss than the sum of their components, the interaction between electrochemical and mechanical processes has been recognized in many works, and they have been referred to as “synergistic” and “additional” effects. The so-called synergistic effect is normally used to describe how corrosion can enhance erosion, while the so-called “additive effect” refers to the mechanism by which erosion can enhance corrosion. In general, the influencing parameters in this process include the solid sand particles by mass, hardness, density, size, shape, velocity, and impact angle; the target material, such as hardness, metallographic structure, strength, ductility, and toughness; and the environment by slurry composition, flow velocity, and temperature.

Khan et al. [32] carried out erosion-corrosion failure analysis of a mild steel nozzle pipe in water-sand flow. They noticed that a mild steel pipe jet nozzle fitted in a direct impact test rig at a Centre for Erosion–Corrosion Research developed many leaks after a few months of use in erosive flow. Perforation leaks were mostly found upstream, and there was also significant wall thinning at the exit portion. They presented thorough results of a failure study on the pipe jet nozzle leakage. Visual observation, energy-dispersive spectroscopy, 3D scanning, scanning electron microscopy, and laser profilometry data were used in the inquiry. Furthermore, numerical simulations using the discrete phase model (DPM) and computational fluid dynamics (CFD) were carried out to inquire into the underlying reasons why there were leaks in the pipe jet nozzle. Three distinct pipe jet designs were subjected to additional CFD-DPM simulations for liquid-solid flow conditions. The results were analyzed in order to identify a different design that would avoid the pipe jet nozzles failing. It was discovered that leaks and cracks in the pipe jet nozzle were caused by the increase in turbulence as well as many particle-impacts on its wall. Furthermore, when the failed pipe was replaced with an alternative nozzle pipe design with a chamfer reducer section, the CFD-DPM revealed a five-fold decrease in the maximum erosion rate. The modified reducer section design was found to have the biggest effect on mitigating erosive wear, according to the CFD-DPM study of all geometric configurations.

Laukkanen et al. [33] undertook the development and validation of a coupled erosion-corrosion model for wear-resistant steels in environments with varying pH. They argued that because of its complexity, modeling efforts have mostly ignored erosion-corrosion, which is the combined loss of material brought on by the combined impacts of particle erosion and electrochemical corrosion. It has been difficult to evaluate how erosion and corrosion work together to cause far larger material losses under extreme circumstances than they would if they worked alone. With differing degrees of success, a number of analytical and semi-empirical approaches have been put forth; yet, it has been a common result that these modeling efforts have not always produced the desired predictive capabilities or transferability. The current work addresses this feature and aims to improve it by introducing a concept that combines the point defect model (PDM) and computational fluid dynamics (CFD) with a wear model that is defined using micromechanical finite elements. The implemented method was used to investigate erosion-corrosion in a stirring tank designed with varying temperature, pH, abrasive particle type, flow velocity, and solution chemistry. A comprehensive characterization regime was conducted in addition to experimental work to provide a dataset for model validation for a wear-resistant steel containing two distinct abrasives, chromite and quartz particles, in order to examine model performance. Model predictions are directly contrasted with the outcomes of the corresponding experiments that represent industrially relevant erosion-corrosion conditions. According to the validation tests, the erosion-corrosion model yields satisfactory results and accurately forecasts the primary trends of the experimental dataset. The introduced erosion-corrosion model's capabilities and approximations are assessed and examined, and the necessity for further improvement is noted.

According to Toor et al. [34], the majority of oil and gas production wells contain a large number of solid particles and corrosive species. In these production conditions, CO_2 gas can dissolve in free-phase water and generate carbonic acid (H_2CO_3). Unpredictable, severe localized CO_2 corrosion and/or erosion-corrosion (EC) can be caused by carbonic acid, fluid movement, and solid particles (sand or other entrained particles). The CO_2 EC performance of API 5L X-65 carbon steel, a material frequently found in numerous oil and gas piping infrastructures, was investigated in a 0.2 M NaCl solution at room temperature, using a recirculation flow loop at three different CO_2 concentrations, with pH values of 4.5, 5.0, and 5.5, two impingement velocities of 8 and 16 m/s, three impingement angles of 15°, 45°, and 90°, and with or without 2000 ppm sand particle concentrations for three hours. FE-SEM, EDS, and XRD were used to characterize the corrosion products. They found that there were more H^+ ions available and observed that CO_2 and EC rates dropped as pH rose. They also found that a 45-degree

impingement angle with solid particles produced the highest rates of CO₂ erosion and corrosion, and a change in pH value had influence on the corrosion resistance and morphology of the corrosion scales.

Sadique et al. [35] reported that the existence of sand in production lines of oil and gas industries causes material degradation due to erosive and corrosive processes, which can lead to costly monitoring and maintenance and significant accident cases. They observed that the process of erosion-corrosion consists of erosion, corrosion, and their interactions, and investigating and understanding how the erosion-corrosion process affects the degradation process in certain materials will allow for a reduction in economic loss and help prevent accidents. In their investigation, they used a submerged impingement jet (SIJ) test to examine material loss resulting from erosion and corrosion of mild steel under the impingement of sand-laden water at a 90° impingement angle. They focused on the effects of jet velocity and sand loading on weight loss owing to erosion alone, weight loss due to erosion-corrosion interactions, and weight loss due to pure erosion at temperatures between 29 and 33 °C in a seawater environment of 3.5% NaCl content. According to the findings of their research, erosion was more prevalent under all tested conditions, and velocity and sand loading had a significant impact on the removal of materials. They also discussed how the impingement test affected the specimen's surface properties.

Abdu et al. [36] conducted erosion-corrosion failure analysis of API X52 steel pipeline. Complete material characterizations were conducted as part of the inquiry utilizing optical microscopy, scanning electron microscopy, energy-dispersive x-ray spectroscopy, and tensile and hardness tests. It was noteworthy to note that the downstream pipe at the welded connection at the elbow outlet, rather than the elbow itself, experienced the primary failure. It was discovered that the primary mechanism of failure was the erosion-corrosion process, which led to the downstream pipe's thinning, the dissolution of the protective FeCO₃ film, and ultimately failure. Sand impingement from turbulent flow, which was encouraged by an abrupt shift in the flow cross section between the elbow inlet and upstream pipe and poor welding quality of the joint at the elbow outlet, is thought to have caused the erosion-corrosion.

Khan et al. [37] noted that erosion and corrosion in flow-changing devices as a result of sand transportation is a serious concern in the hydrocarbon and mineral processing industries, so they investigated the flow-accelerated erosion-corrosion mechanism of 30°, 60°, and 90° long-radius horizontal-horizontal carbon steel elbows with an inner diameter of 50.8 mm in an experimental closed-flow loop. They elucidated erosion and corrosion for these geometrical configurations for erosive slug flow regimes and reported in detail the extent of material degradation. Qualitative techniques such as multilayer paint modelling and microscopic surface imaging were to scrutinize the flow-accelerated erosion-corrosion mechanism. The 3D roughness characterization of the surface indicated that the maximum roughness appeared downstream, adjacent to the outlet of the 90° elbow. The microscopic surface imaging of eroded elbow surfaces showed the presence of corrosion pits on the exit regions of the 60 and 90-degree elbows, but only erosion scars were formed on the entry regions of the 30-degree elbow. The surface characterization and mass loss results indicated that changing the elbow geometrical configuration from a small angle to a large angle significantly changed the mechanical wear mechanism of the tested elbows. They also identified the maximum erosive location at the top of the horizontally oriented elbow for slug flow.

Pasha et al. [38] used a slurry impingement rig containing 6% by weight of SiO₂ particles to investigate the synergistic erosion-corrosion behavior of X-65 carbon steel at various impingement angles. They found that maximum erosion-corrosion and erosion rates occurred at impingement angles of about 25° and 40–55°, respectively. They reported that the synergy value highly depended on the impingement angle. They found that the formation of patches of porous corrosion product followed by the formation of corrosion pits led to a positive synergy under an impingement angle of 25°. At higher impingement angles, the absence of pits, probably due to the formation of a more durable tribo-corrosion layer, resulted in a negative synergy.

Mohammed Nabeel Majeed [39] asserted in his study that in the oil and gas sector, using corrosion-resistant alloys, particularly stainless steels, is thought to be one of the best ways to prevent corrosion in the presence of harsh conditions like carbon dioxide and chloride ions. This is because their surfaces have a thin, protective passive coating that serves as a barrier between the substrate and the corrosive environment around it. However, due to passive film loss caused by sand particle contact, the presence of sand particles in the flowing stream might lessen these alloys' higher corrosion resistance, leaving the substrate exposed to corrosive environments. The term "erosion-corrosion" is frequently used to describe this phenomenon. Given that stainless steels differ in their chemical makeups and mechanical characteristics, the impact of sand particles can also result in notable surface and subsurface alterations, which have a major impact on the steels' resistance to erosion and corrosion. Understanding how these materials will respond to erosion and erosion-corrosion situations is crucial because of this. The impact of static corrosion behavior on stainless steels' resistance to erosion and corrosion as a function of temperature was examined. Additionally, the degradation of stainless steels under erosion and erosion-corrosion circumstances has been discussed, along with the causes that lead to their failure. In addition, the study looked into how impact angles affected the percentage contribution of stainless steel's overall weight loss components. The degradation behavior of the investigated materials under erosion-corrosion conditions was explained by means of gravimetric and electrochemical measurements, as well as post-test surface analysis, which included surface optical profilometry (Bruker-NPFLEX), focused ion beam (FIB), transmission electron microscopy (TEM), scanning electron microscopy (SEM), and micro indentation hardness tests. The erosion-corrosion resistance of stainless steels and their static corrosion behavior have been found to be closely correlated. For instance, there was a strong correlation between erosion-enhanced corrosion and the ability to passivate again under static conditions, that is, at the Eb-Er and maximum current

conditions. Additionally, in erosion-corrosion circumstances, the same characteristics showed a strong correlation with the re-passivation time. Furthermore, the findings showed that the hardness change can be used as a predictor of stainless steels' ability to withstand erosion under harsh circumstances. Additionally, the percentage of the overall weight loss proportion contribution is significantly impacted by the impact angle. Stainless steel's unique erosion-corrosion resistance was determined to be caused by the percentage of corrosion-enhanced erosion contribution.

Elemuren et al. [40] investigated the synergistic erosion-corrosion behavior of AISI 2205 duplex stainless steel elbows in potash brine-sand slurry and the associated microstructural changes. They found that the combined effects of mechanical and electrochemical processes cause slurry erosion-corrosion damage to materials utilized in mineral processing industries. This study used slurries with 10, 20, 30, 40, and 50 weight percent sand particles and saturated potash brine to evaluate AISI 2205 duplex stainless steel elbows in a flow loop. Tests for erosion and corrosion were carried out at 2.5 and 4.0 m/s flow rates. The gravimetric analysis's findings showed that erosion-corrosion rates rose at both velocities as particle concentration rose. The passive oxide deposit on the elbows' surface is responsible for their negative synergy under all operating situations. The degraded surfaces' microstructural analysis revealed that cutting and plastic deformation were the methods used to remove the material. Electron backscattered diffraction analysis indicates that plastic deformation, which occurred around 4 μm below the eroded surface, resulted in the transformation of metastable austenite phase to martensite.

Zheng and Liu [41] studied slurry erosion-corrosion wear behavior in SiC-containing NaOH solutions of Mo_2NiB_2 cermet prepared by reactive sintering. They argued that erosive wear, erosion-corrosion, and the coal-mining sector are examples of slurry flow units that might result in significant rates of material loss, especially in the hydro transport system where corrosive slurries are encountered. Applications for coatings and hard facing for important components where high durability is required are growing. These materials include stainless steel, metal matrix composites (MMCs), and others that consist of a ductile binder with a reinforcing hard phase. This study assesses the erosion-corrosion performance of cermet based on MoNiB that are applied using the reaction sintering technique. Three cermet with different Mo_2NiB_2 phase range volume fractions and a Ni binder have been taken into consideration. Investigations and discussions are held about the microstructure and characteristics of cermet based on MoNiB . Under alkaline conditions, the impact of the Mo_2NiB_2 phase volume fraction on erosion and erosion-corrosion resistance is studied. The findings show that the Mo_2NiB_2 phase accumulates together with the rise in boron percentage. In the meantime, the volume percentage of Mo_2NiB_2 is directly correlated with the hardness. The wear behavior is significantly influenced by the Mo_2NiB_2 phase. The impact of the Mo_2NiB_2 phase volume fraction on the erosion-corrosion of Mo_2NiB_2 -based ceramics that only contain NaOH solution differs from that of erosion that contains both SiC and NaOH solution. Having more Mo_2NiB_2 phase is beneficial for corrosion resistance. The cermet with less Mo_2NiB_2 phase deteriorates mostly owing to corrosion in alkaline slurry impact, which lowers the mechanical characteristics and accelerates the overall loss of material. On the other hand, erosion and corrosion work together to create weight gain in alkaline slurry containing SiC particles. Because of the increased interference between impinging and reflected erodent, corrosive production is the primary source of weight gain when the volume fraction of Mo_2NiB_2 is low. There is more Mo_2NiB_2 phase, more corrosion resistance, and significantly less corrosive output.

Naz et al. [42] developed erosion-corrosion mechanisms for the study of steel surface behavior in a sand slurry. In their work, they used dry sand impact and linear polarization resistance (LPR) monitoring techniques to study the detrimental effects of the sand size on the surface morphology of the mild steel. An electrochemical mechanism was developed to measure the resistance of the metal coupons rotating in a slurry of 4% by weight NaCl and 5% by weight sand. Scanning probe microscopy and hardness testing of the eroded coupons was conducted to elaborate on their surface topography. The in-depth analysis of their research results revealed that not only the larger particles but also the smaller particles caused significant erosion and corrosion of the steel coupons. It was also noticed from the research that the hardness and density of the eroded particles were reasonably high enough to induce plastic deformation and microstructures at the metal surface. LPR measurements revealed higher coupon resistance in the fine sand slurry than in the coarse sand slurry. In addition, the study found that the localized corrosion and erosion-corrosion attacks on the metal surface were also supplemented by the stirring rate and the presence of NaCl in the solution. It was also reported that the corrosion rate sharply increased with an increase in stirring rate above 500 rpm.

Peat et al. [43] studied three high-velocity oxy-fuel-deposited coatings, tungsten carbide, chromium carbide, and aluminum oxide, under slurry erosion-corrosion conditions. This type of coating is suited for usage in extremely erosive and corrosive settings since it usually has a higher density and hardness than other thermal spray technologies. In order to assess the mechanisms producing coating degradation, the study's scope focused on employing metallographic analysis and applied electrochemistry to isolate the relevant factors of erosion, corrosion, and synergy. Its objective is to offer thorough information on how well the aforementioned coatings function under erosion-corrosion circumstances that mimic a flowing environment. The results show that in comparison to the uncoated S355 steel, the breakdown of the aluminum oxide and chromium carbide coatings causes an increased mass loss. In spite of this, the research demonstrated that tungsten carbide with a cobalt binder is a protective coating that significantly reduces overall material loss when compared to S355 steel that is not coated.

Espinoza-Jara et al. [44] contended that engineering systems that operate under particle-laden turbulent flow regimes, such as slurry pumps, are vulnerable to erosive wear, where the specific conditions of particle impingement are decisive for determining the wear rate of the surface under erosion and hence its suitability for the mechanical or hydraulic system. On the other hand, developing and testing experimental and computational models that depict particle movement over the surface is challenging due

to near-wall interactions in turbulent flow processes. Their study examined the consistency of the statistical distributions of particle impact angle and impact direction found in a slurry pot configuration with experimental data obtained from a Large-Eddy Simulation (LES) using the Wall-Adapting Local Eddy-Viscosity (WALE) model of the flow. The impact angle, impact direction, and particle velocity distributions that were obtained from the applied CFD formulation yielded nearly identical characteristic values to those that were obtained from the experimental data. Shorter computation times and validation through comparison with direct simulation are provided by the LES-WALE technique employed in their work. The applicability and prospective dynamic simulation of practical engineering cases with the model were highlighted.

Waldi et al. [45] studied erosion-corrosion simulation of thermally sprayed WC-based cermet in dam water and artificial seawater environments. They contended that mechanical equipment that is operated in a water dam environment is at risk of erosion-corrosion. To tackle the issue, thermally sprayed ceramic coatings are a requisite solution for increasing resistance to corrosion and wear in hydro-turbines, particularly with high river sedimentation loads such as those in Cirata and Jatiluhur dams in Indonesia. In their study, WC-based ceramic coatings of WC-10Co-4Cr and WC-12Co, respectively, were coated on AISI 1030 steel substrate and evaluated in media simulating the Cirata and Jatiluhur water dam environments, as well as in simulated seawater conditions. SEM and XRD were used to examine the morphology and structure of the sprayed coating; surface roughness, porosity, and microhardness were also investigated. Potentiodynamic polarization was used to assess the coating's resistance to corrosion. Coupon tests were used to investigate erosion-corrosion resistance in seawater simulations by closed flow loop system (CFLS) equipment. At 0.06-0.15 mm/year and 0.16-0.26 mm/year, respectively, the results demonstrated that the WC-10Co-4Cr coating has high electrochemical corrosion resistance with less erosion and corrosion than the WC-12Co coating. Because stable WCr_2O_6 and W_18O_49 oxides were formed, coatings with a higher Cr content exhibited a reduced rate of corrosion, which makes them an excellent option for coating hydro turbine components.

Erosion-corrosion behaviors of X65 pipeline steel in the flowing CO_2 -saturated electrolyte were electrochemically studied by Zhang et al. [46] using a rotation disc system. The study results showed that the accumulation of the Fe_3C layer in the electrolyte without sand particles enhanced the cathodic reaction, increasing the corrosion rate. The increase in flow velocity facilitated the rapid accumulation of a thick Fe_3C layer, which linearly increased the corrosion rate with increasing rotation speed. The sand impacts removed the corrosion product layer and broke the exposed Fe_3C network, resulting in a negative synergy of erosion-enhanced corrosion. The erosion-corrosion negatively affected ferrites compared with the pearlites in an electrolyte containing sand due to the weaker erosion resistance.

Liang et al. [47] affirmed that the surface material of marine ship hulls suffers degradation by slurry erosion due to the impact of sands or solid particles in seawater. When the motion speed of the ship increases, there is a sudden change in pressure, and cavitation erosion will occur. Hence, the corrosion of the surface material of the ship hulls in the ocean is a combined damage in slurry erosion and cavitation erosion states. An experimental device capable of simulating the above working conditions for the combined wear was designed and manufactured. A combined wear test of Q235, DH32, and NM360 steels was conducted. Results show that cutting furrows of the slurry erosion, pinholes of the cavitation erosion, holes of electrochemical corrosion, and their combined effect increase the material wear rates and areas. Ductile materials of high strength have less slurry and cavitation damage but more corrosion damage. For ductile materials of low strength, slurry and cavitation wear play an important role. When the slurry impact speed is increased, the wear degree of materials increases as well. The experimental setup for the combined wear has provided strong support for the development of wear-resistant materials for ship hulls and the structural optimization of the hulls.

Shiva Suthan Rajahram [48] carried out a research project with the aim to develop a systematic understanding towards modelling erosion-corrosion by investigating the erosion-corrosion mechanisms of stainless steel UNS S31603. An integrated approach, consisting of three main thrusts from environmental, electrochemical, and material perspective was used in the study. He contended that, "solid particle erosion-corrosion is the wear originated by the combined action of the mechanical process of solid particle erosion and the electrochemical process of corrosion. This joint action leads to synergistic interaction that worsens the wear rate of the material. This causes severe problems to engineering components exposed to these aggressive conditions and poses a problem to designers and engineers, as there are currently no robust models available for predicting erosion-corrosion rates due to the lack of complete understanding of the physical erosion-corrosion mechanisms and synergy". The fundamental part of the research examined the robustness of the semi-empirical model from the basis of an active area principle, which had been developed recently at the University of Southampton on a passive metal UNS S31603. Gravimetric experiments were performed with a slurry pot erosion tester. The pot erosion tester was in addition modified to perform in-situ electrochemical investigations. Results obtained from this novel modification revealed that the erosion-corrosion rates and synergy levels increased with increasing velocity, sand concentration, and temperature. Electrochemical current noise measurements for multiple particle impact experiments revealed this to be partly due to the continuous rupture of the oxide film leading to a worsened erosion in corrosion synergistic effect. The erosion-corrosion rates were found to be dependent on the kinetic energy of the particles and the number and size of the particles impacting the surface. The amount of charge consumed and the passivation kinetics were gotten from the unique particle impact experiments. Lips also appeared to crack on the surface, believed to be caused by corrosive action that accelerated material removal. The results were statistically analyzed, and for the first time, interaction contour plots were used to decouple the interactions between the test parameters. These studies revealed that the largest interaction arose between velocity and sand concentration. Empirical models were further derived from these analyses.

The model furnished reasonable predictions of the synergy values, as the unanswered question of whether the right mechanisms were being modelled formed an important basis for the research work. For the first time, an in-depth investigation was conducted on the evolution of wear on the surface and subsurface of UNS S31603 using SEM, FIB, STEM, and TEM. Investigations showcased that a three-layer grain structure consisting of nanograins, micro-grains, and deformed bulk grains was observed to evolve with time. An explanation was proposed on reasons why the mass loss rates vary at different levels of erosion-corrosion by correlating the subsurface and surface wear with the trend of mass loss rate versus time. TEM investigations also disclosed the formation of numerous fatigue cracks and folding of lips on the surface, credited to be due to strain inflicted during sustained particle impact. Other unique features found from the research results were embedment of erodent fragments and chromium oxide layer as well as strain-induced phase transformation. It is believed that a thin composite structure made up of these elements is formed and enhanced by the formation of lips over this structure. All these factors, in combination with grain refinement and work hardening, improve the process of forming fatigue cracks. This process is then speeded up by corrosion, as evidenced by the increased density of cracks observed in the erosion-corrosion sample as compared to the sample subjected to pure erosion. This is suggested to be one of the foremost synergistic mechanisms between corrosion and erosion that is enlarged on by corrosion. Physical models were developed based on these micro- and nanoscale wear observations to merge the surface and subsurface erosion-corrosion mechanisms. An enhanced physical model to explain the erosion-corrosion mechanisms at the subsurface of UNS S31603 was generated from the research. The research findings are of great assistance to engineers and designers in the subsequent development of erosion-corrosion models and in understanding the synergy between erosion and corrosion.

Sharma et al. [49] contended that slurry erosion-corrosion is a very serious problem for many engineering components used in petrochemical, marine, and agricultural sectors. The detrimental effects of slurry erosion-corrosion greatly lessen the service life and increase the maintenance cost. To curb the effects of slurry erosion and corrosion, high-performance, up-to-date materials are needed. In their work, an equimolar molybdenum-niobium-tantalum-titanium-zirconium (Mo-Nb-Ta-Ti-Zr) high-entropy alloy was developed and its slurry erosion-corrosion behavior investigated. For comparative analysis, the conventionally used stainless steel SS316L was similarly investigated. The detailed microstructural characteristics revealed the existence of a two-phase BC crystal structure in the high-entropy alloy. The major BC phase was principally composed of Ta, Nb, and Mo, with the interdendritic area being rich in zirconium (Zr) and titanium (Ti). The Mo-Nb-Ta-Ti-Zr high-entropy alloy exhibited two times higher hardness than the steel SS316L. The high-entropy alloy displayed 3.5 times higher resistance under slurry erosion-corrosion conditions, but under erosive conditions, it revealed two times better performance than the stainless steel. Analysis of the eroded surface morphology revealed the existence of a mixed ductile-brittle erosion response for the high-entropy alloy. The improved performance of the high-entropy alloy is mostly related to its high hardness and extraordinarily high corrosion resistance. Electrochemical corrosion test results revealed that the developed high-entropy alloy has 80 times lower current density than the SS316L steel. The high-entropy alloy also has higher pitting resistance than the steel, resulting in its lower corrosion rates. The electrochemical impedance spectroscopy (EIS) findings showcased a denser and highly stable protective layer. The results indicated that the high-entropy alloy could be effectively used for impeding the slurry erosion-corrosion and corrosive conditions.

Guma and Ishaya [50] investigated waterjet impingement erosion-corrosion of mild steel, a very important but highly corrosion-prone structural material that is used for various purposes. A natural downward hose-flow of distilled water containing various concentrations of 0–20% analytical-grade hydrochloric acid (HCl) and 0–20% slurry particles of diameter 0.1–1 mm was nozzle-controlled to impinge with flow velocities of 5–25 m/s for eight hours at 45 and 90-degree inclination angles on prepared surfaces of the steel coupons. The weight losses, corrosion penetration rates, and micro-topographical changes of the coupons were used to assess the steel corrosion level. The weight losses and corrosion rates of the steel were found to be significantly higher than the literature values from the pure electrochemical corrosion tests. The obtained weight losses and corrosion rates increased more with sand grain sizes, velocity, and sand loading than with the acidity level of the water and were greater at the 45-degree flow impingement angle than at the 90-degree angle. With a water concentration of 20% HCl, 20% slurry particles of diameter one mm, and a flow velocity of 25 m/s, the maximum corrosion rates of 6.271 and 5.771 mm/yr and weight losses of 124 and 114 mg were obtained at 45 and 90-degree flow impingement angles, respectively. SEM micro-topographical analyses of the most corroded coupons in comparison to the uncorroded coupons showed a number of rough spots, with a greater concentration of them around the center of the coupon surface that was impinged at 90 degrees, while the coupon that was impinged at 45 degrees had sporadic micro-craters of faint reddish-brown appearances on its surface.

Zhao et al. [51] investigated the erosion-corrosion behavior and resistance of the AISI 316 stainless steel under water flow jet impingement. The purpose of their investigation was to understand and document the tribo-corrosive wear of the AISI 316 (UNS S31600) stainless steel under high-speed jet impingement by a sand-liquid, two-phase flow. The steel specimens were surface-characterized, and investigated for wear, weight loss, and electrochemical behaviors. Two different types of sands, silica sand, and sea sand, were used in the experiments to investigate the effects of working time and chloride ions from the sea sand. Results showed that the cumulative weight losses of the specimens increased with time. For the effect of particle size on weight loss, it was found that the weight loss caused by the smallest particles over a three-hour time lapse decreased more slowly than that from other particle sizes. In addition, the weight losses of the specimens increased with decreasing impact angle. Erosion from flowing sea sand caused more weight loss than from flowing silica sand. From electrochemical measurements, specimens that were impinged at a moderate angle of 60° exhibited the best corrosion resistance. Specimens that were subjected to the flowing sea sand had worse corrosion resistance than those that were subjected to flowing silica sand. Specimens that were impinged for a

short time represented a passivation process on the anodic polarization behavior, but the passivation disappeared on the specimens that were impinged for a long time.

According to Liu et al. [52], erosion-corrosion is a major issue in pipeline systems used for oil and gas gathering and transportation; in particular, the elbow is the weak point. The impact of flow velocity on the erosion and corrosion of a 90-degree horizontal elbow was investigated. Weight loss measurement was used to examine erosion and corrosion at various points along a horizontal steel elbow that was passed through with sand slurry at varying speeds. Three-dimensional confocal microscopy was used to characterize the erosion samples, and computational fluid dynamics was employed to describe the distribution and flow patterns of sand particles in the elbow. As the fluid velocity increased from 3.5 to 4.0 m/s, the erosion-corrosion rate was found to increase most. The mechanical effects of the particles and secondary flow were found to increase with increasing particle velocity, which resulted in varying velocity contours in the elbow's cross-sections and, consequently, varying erosion-corrosion rates. The elbow outlet with an axial angle between 75 and 90 degrees showed the highest rate in the outer part at annular angles of 45, 90, and 135 degrees and bottom of the inner part at annular angles of 225, 270, and 315 degrees.

Wang et al. [53] contended that tensile stress and internal surface erosion can both damage pipelines in the oil and gas sector at the same time, causing a greater likelihood of pipeline failure. They sought to understand the effects of tensile stress on erosion-corrosion of X70 pipeline steel as well as building and construction components. In the study, a loop system with a stress loading device was used to examine the combined effects of erosion and tensile stress on the corrosion of X70 pipeline steel. Using finite element simulation analysis, potentiodynamic polarization curve, electrochemical impedance spectroscopy, scanning electron microscopy, and a 3D ultra-depth microscope, the general and localized corrosion under the combination of tensile stress and erosion was thoroughly examined. Results from the study demonstrated that erosion and tensile stress can both independently encourage general corrosion. Furthermore, by decreasing the compactness of the corrosion products layer, speeding up the mass transfer process, and enhancing the steel's reaction activity, tensile stress and erosion can work in concert to reduce general corrosion of steels. This was demonstrated by a changed corrosion current density of $37.54 \mu\text{A}/\text{cm}^2$, which even surpassed the impact of tensile stress ($17.76 \mu\text{A}/\text{cm}^2$). Further observations indicate that while tensile stress may produce stress concentration on corrosion defects, erosion can increase the inside-out diffusion of metal cations in the metastable pit and dilute the pit anolyte for localized corrosion. Thus, erosion exhibits an amplification effect from tensile stress but a reduction of localized corrosion.

Brownlie et al [54] hinted that erosion-corrosion can be a significant issue for engineering components used in the geothermal industry. They carried out a study on the erosion-corrosion behavior of engineering materials used in the geothermal industry. The study evaluated the erosion-corrosion behavior of numerous technical alloys utilized in different geothermal power plant components. The materials that were studied included Ti-6Al-4V, carbon steel, low-alloy steel, three grades of stainless steel, and Ni-Cr alloy (Inconel 625). A submerged 90-degree impinging slurry jet made of silica sand particles dispersed in an acidic aqueous solution with pH of 4 and 3.5% content of NaCl was used for the tests. The impact of hydrodynamic circumstances on the erosion-corrosion behavior of the test materials was evaluated using an upgraded volumetric analysis technique, in-situ potentiodynamic polarization scans, and gravimetric mass losses. The effect of applied cathodic protection was also examined. Post-test metallurgical examination was also conducted via SEM. The results showed the distinct differences between low alloy steels and corrosion-resistant alloys, with the former demonstrating substantial material loss in the low-angle corrosive wear region due to large amounts of corrosion-related damage. Both super austenitic stainless steel (UNS S31254) and Inconel 625 (UNS N06625) exhibited the greatest erosion-corrosion resistance of the test materials, with Inconel 625 demonstrating the greatest resistance to high-angle corrosive wear. The relevance of the findings to material selection and other methods of protection against surface degradation in geothermal power plants was discussed.

Owen et al [55] studied erosion-corrosion interactions of X65 carbon steel in aqueous CO_2 environments. They contended that wear rates in carbon steel oil and gas pipelines can be especially high when sand is present in carbon dioxide (CO_2) corrosion settings. Erosion-corrosion is the wear mechanism that occurs when surfaces are struck by a corrosive fluid that contains solids. It is made up of both erosion and corrosion components, and the interactions between erosion and corrosion improve the overall erosion-corrosion degradation. Their work aimed to investigate the causes of corrosion-enhanced erosion and erosion-enhanced corrosion of carbon steel in the regime. The solution was 60°C , pH 4.7, 2% NaCl, and contained 1000 mg/L of sand particles with an average diameter of $250 \mu\text{m}$. The particles flowed through a submerged impinging jet (SIJ) nozzle at a speed of 20 m/s. To further understand how particle impingement contributes to erosion-enhanced corrosion and corrosion-enhanced erosion, particle impact angles and velocities were estimated on the SIJ sample surface using computational fluid dynamics (CFD). Up to 20% of all erosion-corrosion deterioration was found to be caused by corrosion-enhanced erosion, and investigation using focused ion beam scanning electron microscopy (FIB-SEM) revealed that subsurface cracking and the removal of work hardened layers were the main sources of accelerated degradation. Under the measured conditions, erosion-enhanced corrosion was not substantial.

Kim et al. [56] investigated the impact of aging at 850°C on secondary phase precipitation and the ensuing erosion-corrosion behavior of 25% Cr duplex stainless steels. A 30-minute aging period was considered a boundary aging condition for erosion-corrosion since it produced a current density of 0.8 mA cm^{-2} at 9 m s^{-1} in a jet impingement test and a reactivation current to activation current ratio ($i_r/i_a \times 100$) of 1% in a double loop electrochemical potentiodynamic reactivation test. Furthermore, a criterion for the surface to de-passivate by erosion-corrosion would be the current density response of $\sim 0.8 \text{ mA cm}^{-2}$.

Yi et al. [57] disclosed that critical flow velocity (CFV) is one of the valid parameters to evaluate the erosion-corrosion performances of passive materials. For engineering applications, the CFV comparison for typical passive materials is important. Using the impingement jet apparatus, the CFV values of various stainless steel (SS) types, such as the pearlitic 2Cr13 SS, austenitic 304 SS, 316 SS, 254 SMO SS, and two duplex stainless steels (DSS) (2205 DSS and 2507 DSS), in a 3.5 weight percent NaCl solution that contained 2 weight percent silica sand particles were compared. The CFV was calculated using a variety of techniques, potentiostatic polarization tests, mass loss measurements, and surface roughness measurements. The results of these techniques demonstrated good consistency. The highest CFV was shown by the 254 SMO SS, which was followed by the 2507 DSS, 2205 DSS, 316 SS, 304 SS, and 2Cr13 SS. Comprehensive evaluation based on the critical flow velocity and current density at flow velocity higher than the critical value using potentiostatic polarization tests was found to be more effective and efficient for the material selection for erosion-corrosion than the mass loss method, which is typically time-consuming.

Owen et al. [58] observed that erosion-corrosion degradation in oil and gas pipelines is a significant problem, and a change in flow geometry can significantly enhance rates of degradation. In order to assess the erosion-corrosion of X65 carbon steel along the inner and outer internal portions of the bend in an aqueous carbon dioxide (CO₂)-saturated environment with sand particles, they developed a 3D-printed 90-degree elbow that was integrated into a flow loop. They noted that “it is challenging to design representative geometries that can measure erosion, corrosion, and their synergistic interactions. As of the current time, no designs that successfully incorporate the necessary measuring techniques to ascertain local degradation rates throughout the component have been reported in the literature”. They used gravimetric and electrochemical measurement techniques to quantify degradation rates at various locations in the flow geometry in order to clarify the individual contributions to overall erosion-corrosion degradation rates. Their specimen design also made it possible to perform acoustic emission measurements in order to identify particle impacts. The elbow's design was exhibited, and erosion-corrosion tests were performed at a flow rate of 6 m/s in a CO₂-saturated, pH 4, 60 °C, 2 weight percent NaCl solution with 1000 mg/L of sand particles to ascertain the extent and separate contributions of erosion, corrosion, and erosion-corrosion interactions.

Kuruwila et al. [59] carried out a brief review on the erosion-corrosion behavior of engineering materials and reported that the operating conditions of the machinery and parts utilized in the industrial process determine the sector efficiency. The main problems facing industries are corrosion and erosion. Material loss due to corrosion's detrimental impacts is a consequence of equipment deterioration, and equipment deterioration will lead to plant failure; additionally, it poses a risk to public safety and, from a conservation perspective, may result in the exploitation of existing resources. Equipment replacement raises costs and may eventually force the facility to temporarily shut down. In the majority of industrial applications, protecting surfaces against the damaging effects of corrosion and erosion-corrosion is a major problem. Technological developments offer a multitude of methods to tackle challenging circumstances. The way that technology interacts with the environment must be taken into consideration while choosing it. The negative consequences of erosion-corrosion in the current situation were discussed in the review paper.

Sunday Aribio et al. [60] studied the erosion-corrosion behaviors of the aluminum alloy 6063 hybrid composite. Aluminum alloy 6063 (AA6063) composite with varying proportions of snail-shell ash (SSA) and silicon carbide (SiC) reinforcement was developed by stir-casting. Hardness and erosion-corrosion characteristics of the composite were investigated. Erosion-corrosion behaviors of the composite was studied in a mono-ethylene glycol (MEG)-water environment with 20% v/v of ethylene glycol and 0.1 g/L silica sand particles using a redesigned miniature submerged impinging jet rig. SEM-EDX of the as-cast composites indicated the presence of the particulates distributed in the matrix. The hardness of the aluminum alloy was improved up to a maximum value, with the addition of 7.5 wt.% SiC+7.5 wt.% SSA. However, hardness values declined when 10 wt.% SSA+10 wt.% SiC was used as the reinforcing phase. Erosion-corrosion studies showed that the erosion component dominates the total material loss, with the composite that had the highest hardness displaying better erosion-corrosion resistance. Also, addition of MEG to the slurry resulted in lower erosion-enhanced corrosion and total material loss due to erosion-corrosion. SEM images of the damaged composite showed that the damage mechanism was dominated by plowing and indentation.

The erosion-corrosion assessment of UNS S31600 stainless steel and white cast iron under very acidic circumstances was examined by Karafyllias et al. [61]. They observed that erosion-corrosion mechanisms cause pump components, including liners and impellers, to deteriorate significantly in the mining industry. This reduces the productivity of the mining process and the transportation of mined ores. They also observed that certain mines contain abrasive erodent particles, chlorides, and extremely low pH, all of which accelerate the breakdown of the materials. Stainless steels and white cast irons are two alloy classes that are appealing to those aggressive slurries. Their current study examined the erosion-corrosion performance of UNS S31600 stainless steel and hypoeutectic white cast iron with an austenitic matrix (37 WCI). The angle of impingement was the normal incidence, and the testing device employed the submerged jet approach. The solid/liquid impingement tests were carried out using silica angular sand at pH 0 in an aqueous solution containing 3.5% NaCl. By using surface topography, potentiodynamic methods, cathodic protection (CP), and microscopy, a thorough investigation was produced. After a detailed investigation of the proportionate damage of pure erosion, pure corrosion, and their combined effects, the results showed that 37WCI was superior to UNS S31600. To learn how the erosion-corrosion phenomena impact the performance of the materials in various hydrodynamic zones, the metals were also examined in various areas of the tested surface, and it was found that corrosion, not wear resistance, was a key component of the metals' performance. The corrosion rates of both metals were higher in areas where mechanical damage was more pronounced.

Zhao et al. [62] carried out a study on the effects of laser surface melting on the erosion–corrosion of X65 steel in liquid–solid jet impingement conditions. They noted that steels may become more resistant to erosion and corrosion by the use of laser surface melting (LSM). The impact of LSM on the erosion–corrosion resistance of X65 steel has been evaluated in their study using a submerged jet impingement system with sand and brine under saturated CO₂ conditions. Surface profile data and CFD-simulated findings were used to infer erosion–corrosion rates under various experimental settings. The shape of erosion–corrosion damage was examined using scanning electron microscopy (SEM). The findings demonstrate that LSM can reduce the erosion–corrosion rates at different impact angles. In order to shed light on how laser treatment affects the steel, changes in the microstructure, corrosion behavior, and hardness of X65 steel were examined using optical microscopy, transmission electron microscopy (TEM), and energy-dispersive X-ray (EDX) analysis in addition to electrochemical polarization and hardness distribution measurements.

Medvedovski et al. [63] studied the influence of bronzing on steel performance under erosion–abrasion–corrosion conditions simulating downhole oil production. They observed that erosion–corrosion causes significant damage and failures of production equipment components, such as production tubing and pumping systems, in downhole heavy oil production and oil sand processing. This leads to processing losses, production downtime, and expensive maintenance and replacement costs. To reduce these issues, protective coatings (layers) can be applied to the production components, which are primarily made of low-alloy steels. In their study, the performance of a hard bronzed coating made of two iron boride layers (FeB and Fe₂B) that was obtained by thermal diffusion on carbon steel was compared to that of bare steel under conditions of synergistic erosion, abrasion, and corrosion that mimicked the environment of oil production.

Equipment specifically for wear testing was created and constructed. In this test, steel pony rods revolving and oscillating were mixed with high-velocity erosive flows of water–oil slurries containing silica sand and salts to test the inner surface of tubular sections. Following wear testing, the surfaces of the materials under study were structurally examined, and their profiles were measured. Because of its high hardness, high chemical inertness, dual-layer architecture, and diffusion-induced bonding with the substrate, the iron boride coating outperformed bare carbon steel in abrasion and erosion–abrasion–corrosion conditions. Under the most demanding operating conditions, bronzed steel tubing and casing with inner surface protection can be used with success.

Peat et al. [64] evaluated the synergistic erosion–corrosion behavior of HVOF thermal spray coatings. In their study, three high-velocity oxy-fuel-deposited coatings, aluminum oxide, tungsten carbide, and chromium carbide, under slurry erosion–corrosion conditions were examined. This type of coating is usually suited for usage in extremely erosive and corrosive settings since it usually has a higher density and hardness than other thermal spray technologies. In order to assess the mechanisms producing coating degradation, the study scope focused on employing metallographic analysis and applied electrochemistry to isolate the relevant factors of erosion, corrosion, and synergy with the aim of providing comprehensive data on the performance of the coatings under erosion–corrosion in conditions representing a flowing environment. The results show that compared to the uncoated S355 steel, the breakdown of the aluminum oxide and chromium carbide coatings causes an increased mass loss. In spite of this, research has demonstrated that tungsten carbide with a cobalt binder is a protective coating that significantly reduces overall material loss when compared to S355 steel that is not coated.

Giourntas et al. [65] investigated the influence of metallic matrix on the erosion–corrosion behavior of high chromium cast irons under slurry impingement conditions. The diverse materials that make up chromium cast irons (CCI) include a variety of compositions and microstructures that are frequently selected to provide superior wear resistance. But when cast iron is needed to function in environments where corrosion and wear are factors, problems might occur. In this case, the CCI's composition is typically changed to increase the amount of chromium in the metallic matrix and, consequently, the corrosion resistance that high-Cr stainless steels exhibit. The corrosive wear behavior of martensitic-based, near-eutectic cast iron and austenitic-based hypoeutectic cast iron, along with the related stainless steels, in saline water under solid–liquid submerged jet circumstances was compared in their study. A thorough experimental approach that included assessing the materials' behavior under both free erosion–corrosion and cathodic protection circumstances was used. The method emphasized the intricacies of the mechanical/electrochemical interactions that take place during erosion–corrosion and expanded our understanding of the basic degradation mechanisms under various hydrodynamic settings. The impact of micro-galvanic interactions at phase boundaries was found to be a significant characteristic. The findings' implications for corrosion control techniques and CCI alloy selection were examined.

Yi et al. [66] asserted that one crucial metric for assessing the erosion–corrosion performance of passive materials is the critical flow velocity (CFV) and investigated the effect of impact angle on the critical flow velocity for the erosion–corrosion of 304 stainless steel in simulated sand-containing seawater. The investigation was to understand how impact angles affect CFV behavior to advance our knowledge of the CFV mechanism behind erosion and corrosion. The CFV behavior for 304 stainless steel erosion and corrosion was examined at various impact angles in saltwater that was simulated to contain sand. The potentiostatic polarization test, mass loss measurement, surface roughness assessment, and morphological analysis were the testing techniques. Their findings show that the CFV values are, in order, 15 m/s for impact angles of 30°, 13 m/s for 45°, 13 m/s for 60°, and 13 m/s for 90°. The synergistic action of the normal momentum and the shear momentum, which affects the de-passivation–re-passivation behavior of passive films generated on the metal surface, determines how the CFV values change with

impact angles. The predominant erosion-corrosion mechanism shifts from micro-cutting to plastic deformation as the impact angle increases.

Brownlie et al. [67] studied erosion-corrosion behavior of CoCrFeNiMo0.85 and Al0.5CoCrFeNi complex concentrated alloys produced by laser metal deposition. Two complex concentration alloys (CCAs), CoCrFeNiMo0.85 and Al0.5CoCrFeNi, were formed by laser metal deposition (LMD) onto a stainless-steel substrate, and their corrosion and erosion-corrosion behavior were assessed. The CCAs' performances were contrasted with those of carbon steel (P265GH) and wrought stainless steel (UNS S30403). Using a submerged impingement jet test apparatus, erosion-corrosion testing was carried out using a slurry made of angular silica sand in an aqueous solution of 3.5% NaCl, set to a pH of 4, impinging at 90°. Additionally, electrochemical monitoring was done in solid-liquid, flowing, and quiescent environments. The presence of intermetallic phases (identified by XRD) in CoCrFeNiMo0.85 was shown to have a much higher microhardness than Al0.5CoCrFeNi. Despite the fact that the CoCrFeNiMo0.85 CCA typically showed better durability than the Al0.5CoCrFeNi version, it was found that the hydrodynamic conditions affected the relative performances of the materials under investigation. The intricate relationship between corrosion and the whole erosion corrosion process was a significant component. In fact, the ensuing pure mechanical damage showed fewer clear distinctions between the alloys under investigation when cathodic protection was used. Both CCAs underwent comparable mechanical deterioration mechanisms, as shown by post-test microscopy employing SEM: sliding abrasion at low angles and plastic deformation and microcracking at high angles.

Insights into emerging technologies

Emerging technologies, especially artificial intelligence, have been used to detect and predict corrosion rates. This section highlights the many benefits and possible challenges of artificial intelligence, as well as the technical background of its key branches most applicable to solving erosion-corrosion issues, such as pattern recognition, machine learning, and deep learning, and possible challenges with a few current research studies that demonstrate its application and applicability to erosion-corrosion monitoring and control issues [6].

Artificial intelligence is defined as a machine's ability to mimic human behavior, respond perceptively, solve problems, and make decisions automatically without human interference or with less human interference. Automated planning, natural language processing, vision, general intelligence, knowledge representation, and robotics are among the primary goals of artificial intelligence research. Marine research has made use of a wide range of artificial intelligence disciplines, including machine learning, deep learning, pattern recognition, evolutionary computation, neural networks, expert systems, discriminant analysis, metaheuristic optimization, swarm optimization, video processing, and computer vision. Among those technologies, the most dependable and effective approaches in corrosion engineering are pattern recognition, deep learning, and machine learning. Fig. 25 displays the various intelligence techniques and their correlations [6, 68].

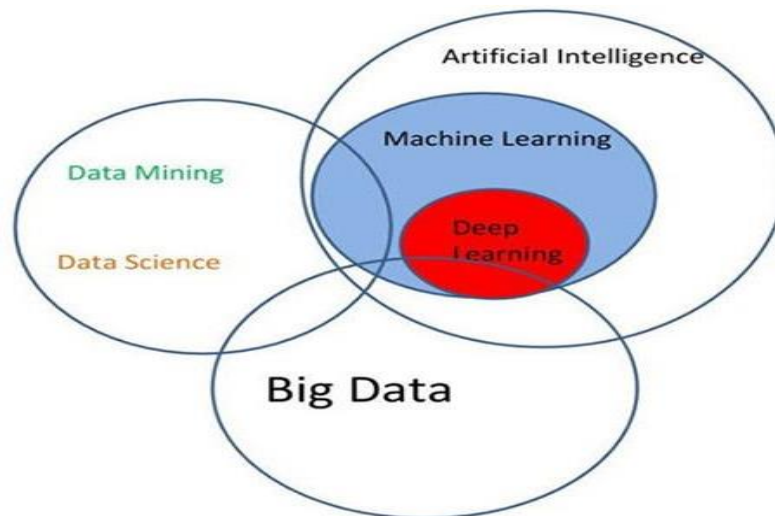


Fig. 25: Artificial intelligence techniques interrelation [6]

Classifying an object into a category or multiple classes is the primary goal of pattern recognition; the objects may be speech, images, handwriting, or signals, depending on the application. Statistical theories are used to establish decision boundaries between pattern classes. The recognition system in pattern recognition has two modes, such as learning (training) and classification. In the training mode, the classifier is trained to partition the feature space after the selection module/feature extraction exposes the appropriate features for representing the input patterns. While the performance of the created classifier, such as the system evaluation module, assesses the classification error rate, input patterns are allocated to one of the classes using the trained classifier. Supervised and unsupervised pattern recognition are the two general categories into which pattern recognition may be divided. Whereas unsupervised pattern recognition lacks labeled training data and no prior knowledge of class level, supervised pattern recognition has access to a set of labeled training samples [68, 69]. Unsupervised pattern recognition is

also called clustering, while a subset of artificial intelligence is machine learning. By mapping environmental factors and alloy composition to corrosion rates, supervised neural networks have been able to predict the corrosion behavior of steel alloys with high accuracy across a variety of corrosion metrics. This highlights the significance of large datasets and sophisticated computational resources for training efficient models. Building and developing mathematical models that can be trained without extensive information is the purpose of machine learning, while enabling informed decision-making is its fundamental goal. Machine learning is used in developing mathematical models that can be taught without fully understanding all of the external influences. Furthermore, by the use of highly developed learning and prediction algorithms, these techniques can facilitate the solution of several issues such as erosion-corrosion problems without or with little human participation with forecast future actions after being taught on provided data. Over the course of a few decades, machine learning models have been successfully applied in a wide range of research domains, including computational finance, image and speech processing, energy production, hydrology, and computational biology. These models have significantly advanced science and engineering as well as improved the quality of our everyday lives. One of the subfields of machine learning is deep learning. In essence, it is a neural network with three or more layers. Although a single layer is capable of making predictions, a second hidden layer helps to increase the accuracy. These neural networks can mimic the human brain and learn from large amounts of data. Numerous fields, including engineering technology application, banking, law enforcement, and customer service, use deep learning technology [6, 68, 69, 70].

In spite of the many advantages of applying artificial intelligence, its implementation to corrosion issues would require specialized, highly skilled workers who must gain relevant experience through prolonged training and possess the fundamental knowledge of artificial intelligence, which is hard to come by. On the other hand, the artificial intelligence itself may experience frequent reliability issues. This may occur if there are numerous flaws and inaccuracies in the models. As a result, the specialists must create and test suitable models and algorithms. Industry flexibility is low, particularly in developing nations. The cheap unskilled labor has been a major component of the industries in many countries. The labor shortage may have an impact on production output. The adaptability of artificial intelligence may be influenced by the high cost of installation and maintenance with the unwillingness of many industries to adapt to it [6, 68].

Application and applicability research outputs on erosion-corrosion

Imran et al. [68] presented a study on the application of artificial intelligence in corrosion monitoring. They said that corrosion is an undesired phenomenon that naturally deteriorates and degrades metallic materials surfaces by chemical and electrochemical reactions with their surroundings. Because it causes metal to fail, leak, and get damaged, it has a big economic impact both now and in the future. Damages amount to billions of dollars annually. It is extremely challenging to detect corrosion with present technology due to the varied boundaries of the corrosion surface and varying textures. Therefore, research into reliable corrosion detection algorithms that work with all levels of corrosion is necessary. The paper first explains the various classes of artificial intelligence and then explains how these applications are used in corrosion monitoring. The review paper's findings contribute fresh and new information to the development of various artificial intelligence techniques that can prevent corrosion-related failures and damages.

Bohane et al. [69], conducted a machine learning-based predictive approach for pitting and uniform corrosion in geothermal energy systems. They observed that although corrosion is a major obstacle, geothermal energy is a renewable source from the earth's crust that has enormous potential for producing electricity. To predict uniform and pitting corrosion, a variety of machine learning models such as support vector regression, k-nearest neighbors, random forest, decision trees, and linear regression were used in their work. When paired with real data, virtual samples from a synthetic data generator produced better results despite minor data performance concerns. Model performance was improved by fine-tuning with several hyperparameters; the decision tree proved to be the most successful. Key parameters impacting uniform and pitting corrosion were identified by exhaustive feature selection, and the models support these findings.

Imran et al. [70] conducted a study on the application of artificial intelligence in marine corrosion prediction and detection. They argued that corrosion, which causes both immediate and long-term consequences, is one of the main issues facing the maritime sector at the moment. Economic losses can be minimized with accurate corrosion monitoring and early forecasts. Conventional methods for predicting and detecting corrosion are laborious and difficult to implement in inaccessible locations. These factors have made algorithms based on artificial intelligence the most widely used research instruments. Their study examines cutting-edge artificial intelligence techniques for predicting and detecting corrosion in marine environments, including computer vision and image processing techniques as well as predictive maintenance techniques. Additionally, a synopsis of artificial intelligence is given. The outcomes of the review are meant to bring forward new knowledge about artificial intelligence and the development of prediction models that can avoid unexpected failures during corrosion detection and maintenance. Moreover, the review was meant to expand our understanding of computer vision and image processing approaches for accurately detecting corrosion in images and videos.

Khalaf et al. [71] conducted a comprehensive review of emerging artificial intelligence technologies for corrosion monitoring in the oil and gas industry. According to them, corrosion poses a serious problem for the oil and gas sector, leading to high maintenance costs and lost output. The accuracy and efficacy of conventional corrosion monitoring approaches are frequently lacking. Nonetheless, the emergence of artificial intelligence in recent years has presented exciting prospects to transform the

corrosion monitoring procedure. In their thorough analysis, they examine several artificial intelligence-powered methods for corrosion monitoring in the oil and gas sector. The review starts by looking at and emphasizing corrosion and the harm it causes to the industry. Second, it explores the variables that affect corrosion, providing a deeper understanding of the intricacy of this process. Third, it looks at how artificial intelligence may be used to create corrosion prediction models, which could help proactively detect and address corrosion-related problems. Fourth, it provides insight into the potential advantages of artificial intelligence technologies for proactive and real-time corrosion detection by illuminating their applications in data analysis, prediction modeling, and monitoring tactics. Lastly, it discusses the difficulties of putting artificial intelligence-driven corrosion monitoring systems for the oil and gas sector into practice. Along with the significance of incorporating human expertise into decision-making processes, topics including data collecting, data quality, algorithm selection, and model validation are covered.

Yan et al. [72] conducted a study on corrosion rate prediction and influencing factors evaluation of low-alloy steels in marine atmospheres using a machine learning approach. They stated that corrosion behavior analysis makes extensive use of empirical modeling techniques. However, modeling objects are frequently restricted to individual elements and particular contexts because of the limited regression capability of standard algorithms. Their work suggested a machine learning-based modeling technique to mimic the behavior of low-alloy steels corroding in maritime environments. Material, environmental, and corrosion rate correlations were assessed, and their effects on steel corrosion behavior were conceptually examined. An optimized random forest model was created with a high prediction accuracy of corrosion rate (R^2 values of 0.94 and 0.73 for the training set and testing set) for various low-alloy steel samples in a number of typical marine atmospheric environments by using the chosen dominating factors as input variables. In a corrosion behavior study, which often entails a regression analysis of several parameters, the results showed that machine learning was effective.

Espinoza-Jara et al. [73] conducted an artificial intelligence-extended prediction of erosion-corrosion degradation of API 5L X65 steel. In contrast to traditional linear regression based on multifactorial analysis (MFA), they claimed that the use of artificial neural networks (ANNs) delivers superior statistical accuracy in erosion-corrosion (E-C) predictions. Due to data scarcity, ANN's limitations—requiring large training datasets and a high number of inputs—present a practical barrier in the field of E-C. They addressed this problem with a unique artificial neural network (ANN) technique that is structured to a limited training dataset and trained using synthetic data to create an E-C neural network (E-C NN). This method was used for the first time in the investigation of E-C wear synergy. By pre-training and fine-tuning the model, transfer learning was used during the process. The first dataset was derived from experimental data obtained by subjecting API 5L X65 steel to a turbulent copper tailing slurry in a slurry pot setup. New experimental data on stand-alone erosion and stand-alone corrosion were added to the previously reported E-C scenario for specific values of flow velocity, particle concentration, temperature, pH, and the amount of dissolved copper ions. E-C NN takes into account both individual characteristics and their interactions when predicting wear loss. The primary finding of the research is that, as indicated by mean squared error (MSE) values of 2.5 and 3.7, respectively, E-C ANN outperforms MFA in terms of prediction. The results were examined in relation to the cross-effect between the E-C NN's improved prediction of the relative contribution to E-C synergy and the suggested predictive model. Using the same experimental dataset, the E-CNN model was found to be a good substitute for MFA, producing predictions that are comparable but more sensitive to E-C synergy at faster computation times.

Chou et al. [74] presented a study on the usability of artificial intelligence combiners for modeling steel pitting risk and corrosion rate. They claimed that corrosion is a frequent degradation that shortens the lifespan of steel and concrete constructions. In particular, corrosion behavior is a very complex problem with many nonlinearities. Advanced artificial intelligence approaches were employed in their work to forecast the marine corrosion rate of carbon steel and the pitting corrosion risk of steel-reinforced concrete. Artificial neural networks (ANNs), support vector regression/machines (SVR/SVMs), classification and regression tree (CART), and linear regression (LR) were the four well-known machine learners that were used to build the single and ensemble artificial intelligence-based models used for prediction. Notably, a hybrid metaheuristic regression model was created by combining a least squares SVR with a smart firefly algorithm, a metaheuristic optimization technique inspired by smart nature. Two datasets from the actual world were used to assess prediction accuracy. With a mean absolute percentage error of 5.6% for pitting corrosion risk and a mean absolute percentage error of 1.26% for marine corrosion rate, the hybrid metaheuristic regression model outperformed the single and ensemble models, according to the comparative results. A viable and useful technique for monitoring corrosion in steel rebar in real time is the hybrid metaheuristic regression model. The hybrid model can be used by civil engineers to plan maintenance procedures that lower the risk of structural failure and maintenance expenses.

V. Conclusion

An up-to-date review of erosion-corrosion from literary sources, covering its origin, affecting factors, impacts, occurrence areas, experimental measuring devices, and research advances, has been conducted. The review demonstrates that:

- i. Erosion-corrosion is mechanically caused action by impinging fluids, usually liquids flowing with velocities above critical values, slurry abrasion, suspended particles in fast-flowing fluids, bubbles, droplets, cavitations, etc., under the synergistic effects of the natural electrochemical corrosion process. The corrosion type is affected by many complex and unpredictable factors, so it is very challenging to accurately find its rates for extending the in-service lives of structural components in fluid flow environments.

- ii. The corrosion type is highly detestable because its rates, time scale, and capacity to deteriorate material components to failure with catastrophic consequences are much more alarming than most other corrosion types. It is a very common corrosion problem in power plants, water, oil, gas, metallurgy, mining, and other industries that utilize mechanical equipment as well as other structural components in hydraulic environments.
- iii. Erosion-corrosion rates are measured using different test rigs of various accuracies, advantages, and disadvantages under classes of jet impingement, slurry pot erosion, pipe flow loop, Coriolis erosion, rotating cylinder apparatus, and in-house devices, with continued search for better devices of accurately measuring its rates. The pot erosion testers are, however, the most commonly used type to date due to their relatively low cost, simplicity, and realistic results for many field applications.
- iv. Erosion-corrosion is a very serious technological and economic problem that has drawn much attention in the last few decades, as attested by so many research outputs on it to date, with a pressing need for better ways of minimizing its impacts. The research outputs are more focused on developing and or testing alternative material components, coatings, and measuring devices for better corrosion resistance and rate measurements under various fluid conditions or situations. Research tests on the corrosion type are usually in accordance with standard procedures such as the ASTM G 76, solid particle erosion-corrosion test standard, and the ASTM G 73, high liquid pressure liquid erosion-corrosion test standard.
- v. Emerging technologies, especially artificial intelligence and machine learning, are employable for precision enhancement and effectiveness in erosion-corrosion monitoring and prediction to overcome the shortcomings of the traditional methods. However, the implementation of such technologies in their attained current sophistication levels in complex corrosion monitoring still presents several challenges that include reliability issues, high costs of upskilling, shortage of relevant skilled workers, higher installation and maintenance costs, and industry willingness to adapt.

References

1. Guma, T.N., Kalu, N.M., Shettima, K.D. and Agbo, S.I. (2023). Corrosivity Extents of Ogororo (locally brewed gin) to aluminum and steel metals and human health implications, *Indian Journal of Engineering, Discovery Scientific Society*, 20, e11ije1011, Doi: <https://doi.org/10.54905/disssi/v20i53/e11ije1011>
2. Guma, T.N., Atiku, S. A., & Abdullahi, A. A. (2017) Corrosion Management and Control: Entrepreneurial Opportunities and Challenges in Nigeria, *International Journal of Engineering Research and Application*, 7(10), 14-23.
3. Azhari, A., Schindler, C., Nkoumbou, J. and Kerscher, E. (2014). Surface Erosion of Carbon Steel 1045 During Waterjet Peening, *Journal of Materials Engineering and Performance*, 23, 1870-1880. DOI: 10.1007/s11665-014-0932-9.
4. Boran Tian. Mechanistic Understanding and Effective Prevention of Erosion-corrosion of Hydro-transport Pipes in Oil Sand Slurry. M.Sc. Thesis, Department of Mechanical and Manufacturing Engineering, University of Calgary, Alberta, Canada, September, 2007.
5. Midany, E.I., Samad, T.T., Menam, A.A.F.A., and Saleh, Y.S.A. (2016). Effect of Particles type, Velocity, and Impact Angle on Slurry Erosion of Stainless Steel Using Simple Test Rig, *Journal of Al Azhar University Engineering Sector*, 11(39), 523-535.
6. Imran, M.M.H., Imran, A.A., Ali, M., Jamaludin, S. and Ayob, A.F.M. The application of artificial intelligence in corrosion monitoring, *Journal of Engineering and Science Research* 7(1), 17-25, 2023
7. Li, P., Zhao, Y. and Wang, L. (2019). Research on Erosion-Corrosion Rate of 304 Stainless Steel in Acidic Slurry via Experimental Design Method, *Materials*, 12, 2330. <https://doi.org/10.3390/ma12142330>
8. Rao, P and Mulky. L. (2023). Erosion-Corrosion of Materials in Industrial Equipment: A Review, *Electrochemical Science Advances*, 10(16), 1-13. <https://doi.org/10.1002/celec.202300152>
9. Javaheri, V., Portera, D. and Kuokkala, V.T. 2018). Slurry erosion of steel-Review of tests, mechanisms and materials, *Wear*, Vols. 408-409, 248-273, <https://doi.org/10.1016/j.wear.2018.05.010>
10. Zadeh, S. A. (2023). Erosion-corrosion. Intech Open. Doi: 10.5772/intechopen.109106
11. Xu, Y., Liu, L., Zhou, Q., Wang, X., Tan, M.Y. and Huang, Y. (2020). An Overview of Major Experimental Methods and Apparatus for Measuring and Investigating Erosion-Corrosion of Ferrous-Based Steels, *Metals*, 10(2), 180, 1-32, <https://doi.org/10.3390/met10020180>
12. Zhao, J., Ma, A., Ji, X., Jiang, J. and Bao Y. (2018) Slurry Erosion Behavior of Al_xCoCrFeNiTi_{0.5} High-Entropy Alloy Coatings Fabricated by Laser Cladding. *Metals*, 8(2), 126. <https://doi.org/10.3390/met8020126>
13. Xu, Y.Z., Liu, L., Xu, C., Wang, X., Tan, M.Y. and Huang, Y. (2020). Electrochemical characteristics of the dynamic progression of erosion-corrosion under different flow conditions and their effects on corrosion rate calculation, *Journal of Solid State Electrochemistry*, 24(2), DOI:10.1007/s10008-020-04795-9.
14. Xu, Y., Liu, L., Zhou, Q., Wang, X., Tan, M.Y. and Huang, Y. (2020). An Overview of Major Experimental Methods and Apparatus for Measuring and Investigating Erosion-Corrosion of Ferrous-Based Steels, *Metals*, 10, 180; 1-32, doi:10.3390/met10020180
15. Buszko, M.H. and Krell, A.K. (2017). Slurry Erosion-Design of test Devices, *Advances in Materials Science*, Vol. 17, No. 2 (52), 1-17, DOI: 10.1515/adms-2017-0007

16. Prabhu, S. Erosion Corrosion: Coatings and Other Preventive Measures, Published: February 22, 2018, by CORROSIONPEDIA. Available online at: <https://www.corrosionpedia.com/2/1868/corrosion-prevention/metallic-and-ceramic-coatings/erosion-corrosion-coatings-and-other-preventive-measures>. Accessed, 23, December, 2024.
17. Roshan, Kuruvila. S., Thirumalai, K. M., Adam, K. and Uthayakumar, M. A brief review on the erosion-corrosion behavior of engineering materials, De Gruyter, Corrosion Review, 2018, 1-12, <https://doi.org/10.1515/corrrev-2018-0022>
18. Kharaji, S. (2023). Self-Healing Coatings. IntechOpen. Doi: 10.5772/intechopen.109500
19. Aljibori, H.S., Alamiery, A. and Kadhum A.A.H. Advances in corrosion protection coatings: A comprehensive review, International Journal of Corrosion Scale Inhibition, 12(4), 2023, 1476-1520, Doi: 10.17675/2305-6894-2023-12-4-6
20. Keshavamurthy, R., Be, N. and Sekhar, N.S. Chapter 10, Thermal Spray Coatings for Erosion-Corrosion Protection, Advances in Chemical and Materials Engineering Books Series, pp. 246-267
21. Selvam Kevin, P., Tiwari, A., Seman, S., Beer Mohamed, S. A. and Jayaganthan, R. (2020). Erosion-Corrosion Protection Due to Cr₃C₂-NiCr Cermet Coating on Stainless Steel. *Coatings*, 10(11), 1042. <https://doi.org/10.3390/coatings10111042>
22. Bisht, A.K., Vaishya, R.O., Walia, R.S. and Singh, G. Nitrides ceramic coatings for tribological applications: A journey from binary to high-entropy compositions, *Ceramics International*, 50(6), 2024, 8553-8585, <https://doi.org/10.1016/j.ceramint.2023.12.245>.
23. Kapali, A., Chitrakar, S., Shrestha, O., Neopane, H.P. and Thapa, B.S. (2019). A Review on Experimental Study of Sediment Erosion in Hydraulic Turbines at Laboratory Conditions, IOP Conference Series: Journal of Physics: Conf. Series 1266 (2019) 012016, IOP Publishing Doi:10.1088/1742-6596/1266/1/012016
24. Saleh, B., Abouel-Kasem, A. and Ahmed, S.M. Effect of Surface Properties Modification on Slurry Erosion–Corrosion Resistance of AISI 5117 Steel, *Journal of Tribology*, 137(3), 2015
25. Gupta, S., Khandelwal, A., Ghose, A. and Chakrabarty, I. (2016). Slurry Erosion Behavior of Destabilized and Deep Cryogenically Treated Cr-Mn-Cu White Cast Irons, *Tribology in Industry*, 486, 486-495.
26. Xu, Y., Zhang, Q., Chen, H. and Huang, Y. (2023). Understanding the interaction between erosion and corrosion of pipeline steel in acid solution of different pH, *Journal of Materials Research and Technology*, Vol. 25, 6550-6566,
27. Aldahash, S.A., Abdelaal, O. and Abdelrhman, Y. (2020). Slurry Erosion–Corrosion Characteristics of As-Built Ti-6Al-4V Manufactured by Selective Laser Melting, *Materials*, 13(18), 3967. <https://doi.org/10.3390/ma13183967>
28. Liu, K., Jiang, W., Chen, W., Liu, L., Xu, Y. Z and Huang, Y.S. (2022). Probing the Dynamic Progression of Erosion–Corrosion of X65 Pipeline Steel Using the Electrical Resistance Method in Conjunction with Galvanostatic Polarization, *Lubricants*, 10(12), 345. 10.3390/lubricants10120345.
29. Salehikahrizangi, P., Raeissi, P., Karimzadeh, F., Calabrese, L. and Proverbi, E. (2021). Effects of Surface Morphology on Erosion–Corrosion and Corrosion Resistance of Highly Hydrophobic Nickel-Tungsten Electrodeposited Film, *Coatings*, 11, 1084, 1-13, 10.3390/coatings11091084
30. Daniel Efirid, K. Flow Corrosion Effects Using Jet Impingement Corrosion Testing. Stress Engineering Service, Inc. Available online at: <https://www.stress.com/flow-corrosion-effects-jet-impingement/>. Accessed 14/09/2020.
31. Selvarajan, R. and Balasubramanian, V. (2018). Corrosion performance of friction surfaced nickel aluminum bronze (NAB) alloy under erosion corrosion and salt fog environment, *Corrosion Engineering, Science and Technology*, 53, 1-6. DOI: 10.1080/1478422X.2018.1425178.
32. Khan, R., Wiczorowski, M., Damjanović, D., Karim, M. R. and Alnaser, I. A. (2023). Erosion-Corrosion Failure Analysis of a Mild Steel Nozzle Pipe in Water-Sand Flow. *Materials*, 16(22), 7084. <https://doi.org/10.3390/ma16227084>
33. Laukkanen, A., Lindgren, M., Andersson, T., Pinomaa, T., & Lindroos, M. (2020). Development and validation of coupled erosion-corrosion model for wear resistant steels in environments with varying pH. *Tribology International*, 151, Article 106534. <https://doi.org/10.1016/j.triboint.2020.106534>
34. Toor, I.U., Alashwan, Z., Badr, H.M., Ben-Mansour, R. and Shirazi, S.A. (2020). Effect of Jet Impingement Velocity and Angle on CO₂ Erosion–Corrosion with and without Sand for API 5L-X65 Carbon Steel. *Materials*, 13, 2198.
35. Sadique, M., Ainane, S., Yap, Y.F., Rostron, P. and Al-Hajri, E. (2017). NaCl Erosion- Corrosion of Mild Steel under Submerged Impingement Jet, *World Academy of Science, Engineering and Technology International Journal of Materials and Metallurgical Engineering*, 11(2), 368-373.
36. Abdu, M.T., Khalifa, W. and Abdelrahman, M.S. Investigation of erosion-corrosion failure of API X52 carbon steel pipeline. *Sci Rep* 13, 20494 (2023). <https://doi.org/10.1038/s41598-023-42556-6>
37. Khan, R., Ya, H.H., Pao, W. and Khan. A. (2019). Erosion-Corrosion of 30°, 60°, and 90° Carbon Steel Elbows in a Multiphase Flow Containing Sand Particles, *Materials*, 12(23), 3898, Doi: 10.3390/ma12233898
38. Pasha, A., Ghasem, H.M. and Neshat, J. (2017). Synergistic Erosion–Corrosion Behavior of X-65 Carbon Steel at Various Impingement Angles, *Journal of Tribology*, 139(1), pp. 1-7, <https://doi.org/10.1115/1.4033336>
39. Mohammed Nabeel Majeed. Understanding the Erosion-Corrosion Behavior of Generic Types of Stainless Steels in a CO₂-Saturated Oilfield Environment, PhD Thesis, University of Leeds, School of Mechanical Engineering, January, 2018

40. Elemuren, R., Evitts, R., Oguocha, I.N.A. *et al.* Synergistic Erosion-Corrosion Behavior of AISI 2205 Duplex Stainless Steel Elbows in Potash Brine-Sand Slurry and the Associated Microstructural Changes. *Journal of Material Engineering and Performance*, 29, 7456–7467 (2020). <https://doi.org/10.1007/s11665-020-05195-w>
41. Zheng, X. and Liu, Y. Slurry erosion–corrosion wear behavior in SiC-containing NaOH solutions of Mo2NiB2 cermets prepared by reactive sintering, *International Journal of Refractory Metals and Hard Materials*, Volume 78, 2019, 193–200, <https://doi.org/10.1016/j.jrmhm.2018.09.017>.
42. Naz, M.Y., Sulaiman, S.A., Shukrullah, S., Ghaffar, A., Ibrahim, K.A., and AbdEl-Salam, N.M. (2017). Development of erosion-corrosion mechanisms for the study of steel surface behavior in a sand slurry, *Measurement*, 106(27), 203-210.
43. Peat, T., Galloway, A.M., Toumpis, A.I. and Harvey, D. Evaluation of the synergistic erosion-corrosion behavior of HVOF thermal spray coatings, *Surface and Coatings Technology*, Volume 299, 2016, 37-48, <https://doi.org/10.1016/j.surfcoat.2016.04.072>.
44. Espinoza-Jara, A., Walczak, M., Molina, V. N. A., Jahn, W. and Brevis, W. (2022). Erosion under turbulent flow: a CFD-based simulation of near-wall turbulent impacts with experimental validation, *Engineering Applications of Computational Fluid Mechanics*. 16, 1526-1545, DOI 10.1080/19942060.2022.2099978.
45. Waldi, M., Leksana, A. M. A., Samudra, H.B., Prajitno, D.H., Syuryana, E.P. and Tjahaya, H. (2023). Erosion-corrosion Simulation of Thermally Sprayed WC-based Cermet in Artificial Seawater and Dam Water Environments, *Engineering Journal*, 27(11), 1-14, DOI:10.4186/ej.2023.27.11.1
46. Zhang, Q., Jiang, W., Wang, Z., Wang, L, Huang, Y. and Xu, Y. (2023). Evaluation of Corrosion and Erosion-Corrosion Behavior of X65 Pipeline Steel in Flowing CO₂-Saturated Electrolyte, *Corrosion*, 79 (6), 587–604.
47. Liang, L., Pang, Y., Tang, Y., Zhang, H., Liu, H. and Li, Y. (2019). Combined wear of slurry erosion, cavitation erosion, and corrosion on the simulated ship surface, *Advances in Mechanical Engineering*, 11(3), 1–14, Doi: 10.1177/1687814019834450
48. Shiva Suthan Rajahram (2010). Erosion-Corrosion Mechanisms of UNS S31603 Stainless Steel. Ph.D. Thesis, Faculty of Engineering, Science and Mathematics, University of Southampton, England, November 2010.
49. Sharma, A., Perumal, G., Arora, H. and Grewal, H. (2021). Slurry Erosion–Corrosion Resistance of MoNbTaTiZr High Entropy Alloy, *Journal of Bio- and Tribo-Corrosion*, 7(3), DOI: 10.1007/s40735-021-00530-7.
50. Guma, T.N. and Ishaya, D.D. (2024). Evaluation of Water Jet Impingement Erosion–Corrosion of Mild Steel under Experimental Operating Conditions, *Academy Journal of Science and Engineering*, 18(2), 101-124.
51. Zhao, Y., Zhou, F., Yao, J., Dong, S. and Li, N. (2015). Erosion–corrosion behavior and corrosion resistance of AISI 316 stainless steel in flow jet impingement, *Wear*, Vols. 328–329, 464-474, <https://doi.org/10.1016/j.wear.2015.03.017>.
52. Liu, J., BaKeDaShi, W., Li, Z., Xu, Y., Ji, W., Zhang, C., Cui, G. and Zhang, R.Y. (2017). Effect of flow velocity on erosion–corrosion of 90-degree horizontal elbow, *Wear*, Vols. 376–377, Part A, 516-525, <https://doi.org/10.1016/j.wear.2016.11.015>.
53. Wang, W., Hu, J. Yuan, X., Zhou, L., Yu, J., Zhang, Z. and Zhong, X. (2022). Understanding the effect of tensile stress on erosion-corrosion of X70 pipeline steel, *Construction and Building Materials*, Vol. 342, Part B, 127972, <https://doi.org/10.1016/j.conbuildmat.2022.127972>.
54. Brownlie, F., Hodgkiess, T., Pearson, A. and Galloway, A.M. (2021). A study on the erosion-corrosion behavior of engineering materials used in the geothermal industry, *Wear*, Vol. 477, 203821, <https://doi.org/10.1016/j.wear.2021.203821>.
55. Owen, J., Ramsey, C., Barker, R. and Neville, A. (2018). Erosion-corrosion interactions of X65 carbon steel in aqueous CO₂ environments, *Wear*, Vols. 414–415, pp. 376-389, <https://doi.org/10.1016/j.wear.2018.09.004>.
56. Kim, Y.J., Kim, S.W., -Kim, H.B., Park, C.N., Choi, Y. and Park, C.J. (2019). Effects of the precipitation of secondary phases on the erosion-corrosion of 25% Cr duplex stainless steel, *Corrosion Science*, Vol.152, pp. 202-210, <https://doi.org/10.1016/j.corsci.2019.03.006>.
57. Yi, J.Z., Hu, H. X., Wang, Z.B. and Zheng, Y.G. (2018). Comparison of critical flow velocity for erosion-corrosion of six stainless steels in 3.5 wt.% NaCl solution containing 2 wt.% silica sand particles, *Wear*, Vols. 416-417, pp. 62-71, <https://doi.org/10.1016/j.wear.2018.10.006>.
58. Owen, J., Ducker, E., Huggan, M., Ramsey, C., Neville, A. and Barker, R. (2019). Design of an elbow for integrated gravimetric, electrochemical and acoustic emission measurements in erosion-corrosion pipe flow environments, *Wear*, Vols. 428-429, pp. 76-84, <https://doi.org/10.1016/j.wear.2019.03.010>.
59. Kuruwila, R., Thirumalai Kumaran, S., Khan, M. & Uthayakumar, M. (2018). A brief review on the erosion-corrosion behavior of engineering materials. *Corrosion Reviews*, 36(5), 435-447. <https://doi.org/10.1515/corrrev-2018-0022>
60. Aribo, S., Fakorede, A., Ige, O. and Olubambi, P. (2017). Erosion-corrosion behavior of aluminum alloy 6063 hybrid composite, *Wear*, Vols. 376–377, Part A, pp. 608-614, <https://doi.org/10.1016/j.wear.2017.01.034>
61. Karafyllias, G., Galloway, A. and Humphries, E. (2021). Erosion-corrosion assessment in strong acidic conditions for a white cast iron and UNS S31600 stainless steel, *Wear*, Vols. 484-485, 203665, <https://doi.org/10.1016/j.wear.2021.203665>.
62. Zhao, W., Wang, C., Zhang, T., Yang, M., Han, B., Neville, A. (2016). Effects of laser surface melting on erosion–corrosion of X65 steel in liquid–solid jet impingement conditions, *Wear*, Vols. 362-363, 39-52, <https://doi.org/10.1016/j.wear.2016.05.006>.

63. Medvedovski, E., Leal Mendoza, G. and Vargas, G. (2021). Influence of Boronizing on Steel Performance under Erosion-Abrasion-Corrosion Conditions Simulating Downhole Oil Production. *Corrosion and Materials Degradation*, 2(2), 293-324. <https://doi.org/10.3390/cmd2020016>,
64. Peat, T., Galloway, A.M., Toumpis, A.I. and Harvey, D. (2016). Evaluation of the synergistic erosion-corrosion behavior of HVOF thermal spray coatings, *Surface and Coatings Technology*, Vol. 299,37-48, <https://doi.org/10.1016/j.surfcoat.2016.04.072>.
65. Giourntas, L., Brownlie, F., Hodgkiess, T. and Galloway, A.M. (2021). Influence of metallic matrix on erosion-corrosion behavior of high chromium cast irons under slurry impingement conditions, *Wear*, 477,203834, <https://doi.org/10.1016/j.wear.2021.203834>.
66. Yi, J., He, S., Wang, Z. et al (2021). Effect of Impact Angle on the Critical Flow Velocity for Erosion–Corrosion of 304 Stainless Steel in Simulated Sand-Containing Sea Water. *J. Bio Tribo Corros* 7, 99. <https://doi.org/10.1007/s40735-021-00538-z>
67. Brownlie, F., Hodgkiess, T. and Fanicchia, F. (2021). Erosion-corrosion behavior of CoCrFeNiMo0.85 and Al0.5CoCrFeNi complex concentrated alloys produced by laser metal deposition, *Surface and Coatings Technology*, Vol. 423, 127634, <https://doi.org/10.1016/j.surfcoat.2021.127634>
68. Imran, M.M.H., Imran, A.A., Ali, M., Jamaludin, S. and Ayob, A.F.M. The application of artificial intelligence in corrosion monitoring, *Journal of Engineering and Science Research* 7 (1): 17-25, 2023
69. Bohane, P., Gohil, T.B. and Srivastav, A.K. Machine learning-based predictive approach for pitting and uniform corrosion in geothermal energy systems, *Electrochimica Acta*, Volume 504, 2024, 144884, <https://doi.org/10.1016/j.electacta.2024.144884>.
70. Imran, M.M.H., Jamaludin, S., Ayob, A.F.M., Ahmad Ali Imran Mohd Ali, A.A.I.M., Sayyid Zainal Abidin Syed Ahmad, S.Z.A.S., Akhbar, M.F.A., Suhrab, M.I.R., et al. Application of Artificial Intelligence in Marine Corrosion Prediction and Detection, *Journal of Marine Science and Engineering*, 2023, № 2, p. 256, <https://doi.org/10.3390/jmse11020256>
71. Khalaf, A.H., Xiao, Y., Xu, N., Wu, B., Li, H., Lin, B., Nie, Z. and Tang, J. Emerging AI technologies for corrosion monitoring in oil and gas industry: A comprehensive review, *Engineering Failure Analysis*, Volume 155, 2024, 107735, <https://doi.org/10.1016/j.engfailanal.2023.107735>.
72. Yan L, Diao Y, Lang Z, Gao K. Corrosion rate prediction and influencing factors evaluation of low-alloy steels in marine atmosphere using machine learning approach. *Sci Technol Adv Mater*. 2020 Jun 19;21(1):359-370. doi: 10.1080/14686996.2020.1746196. PMID: 32939161; PMCID: PMC7476538
73. Espinoza-Jara, A., Wilk, I., Aguirre, J. and Walczak, M. (2023). An AI-Extended Prediction of Erosion-Corrosion Degradation of API 5L X65 Steel. *Lubricants*, 11(10), 431. <https://doi.org/10.3390/lubricants11100431>
74. Chou, J., Ngo, N. and Chong, W.K. The use of artificial intelligence combiners for modeling steel pitting risk and corrosion rate, *Engineering Applications of Artificial Intelligence*, Volume 65, 2017, Pages 471-483, <https://doi.org/10.1016/j.engappai.2016.09.008>.